Biogeosciences, 21, 4495–4519, 2024
https://doi.org/10.5194/bg-21-4495-2024

Biogeosciences Open Access EGU

Seasonal dynamics and regional distribution patterns of CO_2 and CH_4 in the north-eastern Baltic Sea

Silvie Lainela[1], Erik Jacobs[2], Stella-Theresa Luik[1,i], Gregor Rehder[2], and Urmas Lips[1]

[1]Department of Marine Systems, Tallinn University of Technology, Tallinn, 12618, Estonia
[2]Leibniz Institute for Baltic Sea Research Warnemünde, Rostock, 18119, Germany
[i]previously published under the name Stella-Theresa Stoicescu

Correspondence: Silvie Lainela (silvie.lainela@taltech.ee)

Received: 8 March 2024 – Discussion started: 13 March 2024
Revised: 22 June 2024 – Accepted: 23 July 2024 – Published: 15 October 2024

Abstract. Significant research has been carried out in the last decade to describe the CO_2 system dynamics in the Baltic Sea. However, there is a lack of knowledge in this field in the NE Baltic Sea, which is the main focus of the present study. We analysed the physical forcing and hydrographic background in the study year (2018) and tried to elucidate the observed patterns of surface water CO_2 partial pressure (pCO_2) and methane concentrations (cCH_4). Surface water pCO_2 and cCH_4 were continuously measured during six monitoring cruises onboard R/V *Salme*, covering the Northern Baltic Proper (NBP), the Gulf of Finland (GoF), and the Gulf of Riga (GoR) and all seasons in 2018. The general seasonal pCO_2 pattern showed oversaturation in autumn–winter (average relative CO_2 saturation 1.2) and undersaturation in spring–summer (average relative CO_2 saturation 0.5), but it locally reached the saturation level during the cruises in April, May, and August in the GoR and in August in the GoF. The cCH_4 was oversaturated during the entire study period, and the seasonal course was not well exposed on the background of high variability. Surface water pCO_2 and cCH_4 distributions showed larger spatial variability in the GoR and GoF than in the NBP for all six cruises. We linked the observed local maxima to river bulges, coastal upwelling events, fronts, and occasions when vertical mixing reached the seabed in shallow areas. Seasonal averaging over the CO_2 flux suggests a weak sink for atmospheric CO_2 for all basins, but high variability and the long periods between cruises (temporal gaps in observation) preclude a clear statement.

1 Introduction

Carbon dioxide (CO_2) and methane (CH_4) are important atmospheric greenhouse gases influencing the global climate. Changes in the levels of these trace gases are monitored in comparison with the pre-industrial era; however, precise and systematic atmospheric CO_2 and CH_4 measurements were not started before the late 1950s and early 1980s, respectively (Keeling et al., 2009; Dlugokencky et al., 1994). In the recent decade (2012–2021), the atmospheric CO_2 growth rate was 5.2 ± 0.02 GtC yr^{-1} (Friedlingstein et al., 2022). Atmospheric concentration of CH_4 remained nearly constant from the late 1990s through 2006 but resumed increasing since then at an average rate of 7.6 ± 2.7 ppb yr^{-1} estimated for 2010–2019 (Canadell et al., 2023). Methane has large emissions from both natural (e.g. wetlands) and anthropogenic (e.g. enteric fermentation, manure treatment, fossil fuel exploitation) sources, but a clear demarcation of their nature is difficult (Canadell et al., 2023).

The global ocean is estimated to be a net sink of CO_2 (26 % of total CO_2 emissions during the decade 2012–2021; Friedlingstein et al., 2022). However, these global estimates are only beginning to resolve the net CO_2 source–sink characteristics of the coastal ocean. The complexity of processes in the coastal ocean and the limited data availability make it difficult to quantify regional carbon budgets and the coastal ocean's role in the global carbon budget. Although oceanic methane emissions play a modest role in the global methane budget (Reeburgh, 2007), estuaries and other coastal areas contribute up to 75 % of all oceanic CH_4 emissions (Bange

et al., 1994), with an important but not well-quantified contribution of very shallow waters (Borges et al., 2016).

The exchange at the air–sea interface is controlled by the air–sea difference in gas concentrations (CO_2 or CH_4) and by the efficiency of the transfer processes. In the Baltic Proper, the seasonal cycle of CO_2 is characterized by changing saturation levels between different seasons: oversaturation during autumn and winter and considerable undersaturation during spring and summer (Thomas and Schneider, 1999). Spring and summer periods are characterized by two distinct minima attributed to the spring phytoplankton bloom and the cyanobacteria bloom in midsummer, respectively (Schneider et al., 2014; Schneider and Müller, 2018). Understanding the surface water CO_2 dynamics in the Baltic Sea is becoming increasingly important since it is tightly linked to the biogeochemical processes, including primary production and nutrient (nitrogen and phosphorus) dynamics. In addition to the exchange at the air–sea interface and biological processes, the CO_2 system of surface waters in the Baltic Sea is influenced by the changes in hydrological and hydrographic conditions, e.g. river discharges, waves, currents, salinity and temperature, vertical stratification and mixing, upwelling and downwelling, and fronts (e.g. Müller et al., 2016; Jacobs et al., 2021).

Methane is formed by microbial methanogenesis during the decomposition of organic material. CH_4 generated in the sediments that is not consumed at the sediment–water interface can diffuse into the water column and be transported over large areas of the Baltic Sea (e.g. Gülzow et al., 2014). CH_4 is consumed while approaching the surface water due to methane oxidation at the redoxcline and in the oxygenated water column above (Schmale et al., 2010; Jakobs et al., 2013, 2014). This leads to strong vertical stratification with elevated concentrations in the sub-redoxcline layer and concentrations near atmospheric equilibrium at the sea surface (e.g. Schmale et al., 2010). Methanogenesis is generally more prevalent in shallower coastal regions due to the higher organic matter content (Valentine, 2002). In coastal areas, the dominant controlling factors for the seasonal variations in methane emission are the sediment organic matter content (Heyer and Berger, 2000), which might be modulated by seasonal deposition of fresh organic material from primary production, and temperature (Borges et al., 2018). In areas where the water column is relatively shallow and constantly mixed, CH_4 may escape into the atmosphere more readily. In general, the Baltic Sea is a source of atmospheric CH_4 (Bange et al., 1994; Gülzow et al., 2013), with the majority of methane emissions coming from shallow coastal areas (e.g. Roth et al., 2022). Outgassing can be intensified as a consequence of high water temperatures (Humborg et al., 2019) and processes driving vertical transport and mixing, e.g. upwelling events (Jacobs et al., 2021). Production in the upper, oxygenated water column might also contribute to or even govern methane sea–air fluxes (Schmale et al., 2018; Stawiarski et al., 2019), but it is of minor importance in the coastal ocean (Weber et al., 2019) and negligible in shallow coastal areas of high methane concentrations and emissions.

This work is the first extensive trace gas (CH_4 and CO_2) study in the north-eastern Baltic Sea area, with the main focus being on the southern Gulf of Finland (GoF) and the Gulf of Riga (GoR), allowing the assessment of surface layer trace gas and carbon system dynamics in the region. The main aim of our work is to describe the spatial variability and seasonal dynamics of CO_2 and CH_4 and compare these patterns with the better-studied Northern Baltic Proper (NBP) (Schneider et al., 2014; Schneider and Müller, 2018; Jakobs et al., 2014; Gülzow et al., 2013). We analysed the physical forcing and hydrographic and biological background in the study year (2018) and made an effort to link the observed patterns of CO_2 and CH_4 to these drivers.

The questions we try to answer are as follows. Is the seasonal cycle of CO_2 and CH_4 in the southern GoF and GoR similar to that in the NBP? Can we elucidate regional differences in CO_2 and CH_4 dynamics due to river discharges, water depth and mixing, fronts and upwelling events, or other hydrographic features? Do the regional variations in CO_2 and CH_4 dynamics result in differences in yearly fluxes of these gases between the sub-basins? Our analysis is based on measurements during six reoccurring cruises of the Estonian monitoring programme in the north-eastern Baltic Sea (Fig. 1).

2 Study area

The Baltic Sea is a brackish, semi-enclosed sea in northern Europe. High freshwater runoff from the catchment area and sporadic saline water inflows from the North Sea maintain horizontal gradients and vertical stratification (e.g. Leppäranta and Myrberg, 2009). A quasi-permanent halocline exists at depths of 60–70 m in the deeper basins, and a seasonal thermocline develops at depths of 10–20 m from spring to autumn. The present study covers the following Baltic Sea sub-basins (Fig. 1): the NBP (we also include within this a small fraction of the eastern Gotland Basin), the GoF, and the GoR.

The Northern Baltic Proper is the deepest sub-basin, with a maximum depth of about 200 m and very variable topography and coastline. The quasi-permanent halocline separates oxygenated waters in the upper layers and hypoxic and anoxic waters below the halocline. However, no quasi-stationary horizontal gradients of environmental parameters exist in the surface layer. The general circulation pattern in the surface layer is considered mostly cyclonic (e.g. Placke et al., 2018). However, the presence of the northward boundary current along the eastern coasts depends on local wind patterns, and as a consequence downwelling and (less often) upwelling events and associated mesoscale currents may occur (Liblik et al., 2022).

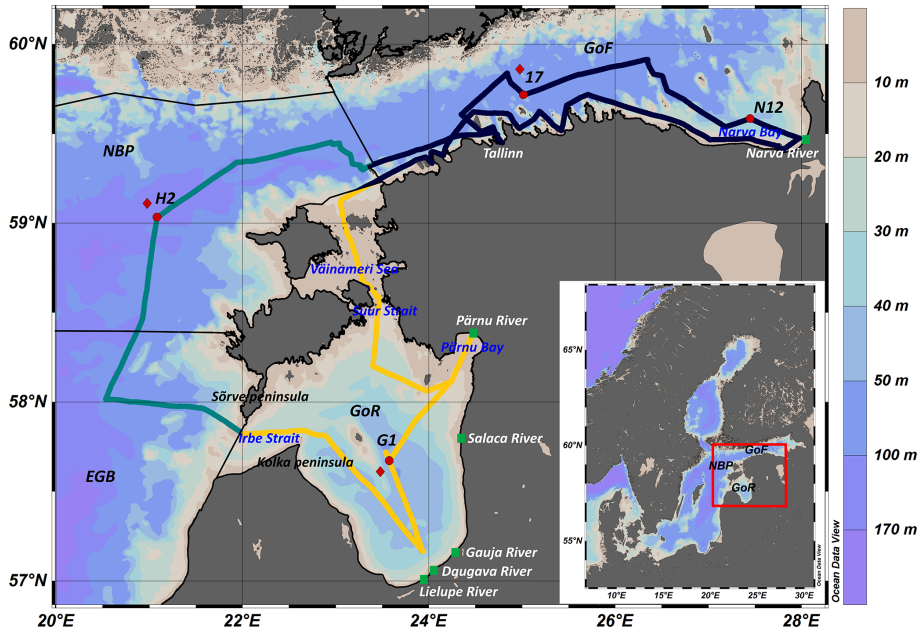

Figure 1. Map of the study area with bottom topography. GoF stands for Gulf of Finland (blue cruise track), NBP stands for Northern Baltic Proper (green), and GoR stands for Gulf of Riga (yellow) (according to HELCOM sub-basin division, marked with black lines). Green-filled squares denote river runoffs. Red-filled circles represent the locations of the most characteristic stations of the sub-basins. Red-filled diamonds denote the closest meteorological ERA5 data grid points to the most characteristic stations of each sub-basin. This map was generated using Ocean Data View (Reiner Schlitzer, Ocean Data View, https://odv.awi.de/, last access: 28 June 2023, 2022).

The Gulf of Finland is an elongated basin (length about 400 km, width varies between 48 and 135 km) with a mean depth of 37 m (depths > 100 m in the western gulf). Due to the direct connection to the NBP in the west and the largest freshwater discharge in the eastern end (Neva River), surface layer salinity decreases from about 6–7 g kg^{-1} at the entrance area to < 2 g kg^{-1} in the easternmost area (e.g. Alenius et al., 1998). During winter, the waterbody is mixed fully in the shallower areas and down to the depth of the quasi-permanent halocline in deeper areas (Alenius et al., 2003). Hypoxic conditions are often observed below the halocline in the deeper areas (e.g. Stoicescu et al., 2019). General circulation in the surface layer is classically considered to be cyclonic (Andrejev et al., 2004) but could be seasonally variable (Maljutenko and Raudsepp, 2019). Energetic mesoscale features, i.e. eddies, fronts, upwelling events, etc. (Pavelson, 2005; Lips et al., 2016a; Kikas and Lips, 2016), may frequently occur. The largest freshwater source along the research vessel (R/V) track analysed in the present study is the Narva River in the south-eastern GoF. Depending on the seasonally varying runoff and local wind conditions, the river water spreads towards the open sea or along the coast and mixes with the gulf water masses (Laanearu and Lips, 2003).

The Gulf of Riga is a semi-enclosed shallow basin with a mean depth of 26 m (Ojaveer, 1995), and the maximum depth of the central basin of 56 m (Stiebrins and Väling, 1996). Freshwater discharge originates mostly from five larger rivers (Daugava, Lielupe, Gauja, Pärnu, and Salaca) in the southern and eastern parts of the gulf (Yurkovskis et al., 1993). Saltier waters from the Baltic Proper enter the gulf via the Irbe Strait in the west (about 70 %–80 % of water exchange) and the Suur Strait in the north (Astok et al., 1999). The whole-basin circulation in the surface layer depends on the prevailing wind pattern, which is mostly cyclonic but anti-cyclonic in summer (Lips et al., 2016b). Anti-cyclonic circulation could also prevail in the southern gulf, connected to the discharges from the Daugava and Lielupe rivers (Soosaar et al., 2016). Due to the shallowness of the basin, the water column is fully mixed in autumn–winter. Thermal stratification starts to develop in April and decays in October–December, depending on the water depth and yearly variable meteorological conditions (Skudra and Lips, 2017; Stoicescu et al., 2022). Near-bottom seasonal hypoxia can be observed in the deeper areas of the central gulf (Stoicescu et al., 2022).

The research vessel track reached the southern gulf close to the largest river discharges (Daugava and Lielupe) and Pärnu Bay, which is shallow and under the influence of the Pärnu River discharge. The measurements were also conducted in the Väinameri Sea, which is the shallow and sheltered sea area (average depth of 5–10 m) between the mainland and the western Estonian islands.

3 Material and methods

The spatial variability and seasonal dynamics of CO_2 and CH_4 in three sub-basins of the north-eastern Baltic Sea in the study year are characterized here. The results are analysed considering the background meteorological and hydrographic conditions, e.g. upper mixed layer (UML) temperature and depth, bottom depth vs. UML depth, fronts and upwelling events, and seasonal and spatial patterns of Chl *a* distribution in the surface layer. CO_2 and CH_4 fluxes are also estimated for all studied areas. Measurement approaches, additional data sources, and calculation methods are described below.

3.1 Meteorological information

Meteorological conditions were evaluated by ERA5 comprehensive reanalysis data (from Copernicus Climate Data Store; Hersbach et al., 2019). Surface net solar radiation, air temperature at 2 m above the sea surface, and winds at 10 m above the sea surface were extracted for the positions closest to the monitoring stations 17, G1, and H2 in the GoF, GoR, and NBP, respectively (see Fig. 1). For the comparison of the study year (2018) and the long-term (1979–2018) meteorological conditions, ERA5 data at station NBP were used. Monthly average reanalysis values in 2018 are presented against the long-term monthly averages and variability, characterized by standard deviations and minimum and maximum values. Average wind vectors and wind roses were calculated for the selected stations in the GoF, GoR, and NBP (Fig. 1) for the cruise periods using 2018 hourly reanalysis data. The presented wind characteristics during the cruises represent 7 d periods ending at the cruise termination date, i.e. periods containing 1–2 d before the cruise up to its end.

3.2 Continuous surface water measurements aboard R/V *Salme*

The measurements were conducted using a flow-through system (Ferrybox) onboard R/V *Salme* during six monitoring cruises in 2018: on 8–12 January, 16–20 April, 28 May–2 June, 9–13 July, 22–27 August, and 22–28 October. The Ferrybox by Go-systemelektronik was equipped with an SBE38 sensor for temperature, an SBE45 MicroTSG sensor for temperature and conductivity, WetLabs *ECO* FL and Turner Design Cyclops-7 sensors for chlorophyll *a* fluorescence, and a digital optode by PONSEL for dissolved oxygen measurements. The Ferrybox water intake was located at a depth of 2 m. The sampling interval was 1 min, corresponding to a nominal spatial resolution of about 250 m while the vessel was moving with its normal cruising speed of 8–9 kn.

The Ferrybox was supplemented with the equipment for trace gas (CO_2 and CH_4) measurements using an equilibrator setup. During the first cruise in January, a LI-COR 6262 CO_2/H_2O instrument coupled to the headspace of a glass equilibrator (similar to Gülzow et al., 2011) was used. During the other cruises, the setup was similar to the MESS presented in Sabbaghzadeh et al. (2021) using a Los Gatos Research CH_4/CO_2 analyser but with a lower water flow of around 2.5–4.5 L min^{-1}. In July and October, the *e*-folding response times of the setup were exemplarily determined to be 720 and 790 s for CH_4 and 35 and 52 s for CO_2; the lower values in July illustrate the influence of higher water temperature (ca. 18 °C vs. 12.5 °C) and higher water flow (ca. 3.6 L min^{-1} vs. 3.1 L min^{-1}). Apart from January, an additional Microx 4 oxygen meter PSt7 optode measured dissolved oxygen in the water supply line of the equilibrator.

Atmospheric pressure was measured during the entire cruise, and measurements of atmospheric CO_2 and CH_4 (as mole fractions in ppm or ppb) were performed one to two times per cruise. For this, the gas supply of the trace gas analyser was switched from the equilibrator to a long tubing used to sample air on the windward side of the upper deck.

The data series contain surface layer temperature, salinity, chlorophyll *a* concentration (Chl *a*), partial pressure of CO_2 (pCO_2), dissolved oxygen concentration, and concentration of CH_4 (cCH_4) with a spatial resolution of about 250 m along the cruise tracks with a length of about 1500 km each, covering three Baltic Sea sub-basins.

3.3 Quality assurance and processing of continuous flow-through data

A two-step calibration procedure was followed for the Ferrybox Chl *a* fluorescence data. First, a linear regression was found between Chl *a* fluorescence data from the conductivity–temperature–depth (CTD) (Ocean Seven 320*plus*, Idronaut s.r.l., with Seapoint fluorometer) and Chl *a* concentrations determined in the laboratory from the water samples collected at respective stations and depths. Chl *a* concentration in the laboratory was determined optically by spectrophotometry (HELCOM, 2017). Afterwards, a linear regression between the calibrated Chl *a* data from CTD at 2 m depth and Ferrybox Chl *a* fluorescence data was found. This calibration procedure was performed separately for each cruise.

The same two-step calibration procedure was used for dissolved oxygen measurements during the cruises in January and April. Dissolved oxygen concentrations from water samples were determined electrochemically using a dissolved oxygen meter (OX 400 1 DO analyser; WWR International, LCC) and also taking into account a salinity correction. For other cruises, the Microx 4 oxygen meter PSt7 optode data were used. Oxygen partial pressures (pO_2) from the PSt7 optode were post-calibrated using discrete sample measurements conducted at 1 m depth at monitoring stations. The procedure was followed separately for each cruise, assuming that the first and last discrete measurements were representative of the start and end of each cruise.

Measured CO_2 and CH_4 mole fractions (xCO_2/xCH_4) were post-calibrated using a near-atmospheric standard gas (398.49 ppm CO_2, 1.91 ppm CH_4, matrix: ambient air). These target measurements were performed at the beginning and end of each cruise and almost every day at sea to achieve a drift correction if necessary. Measured xCO_2 and xCH_4 were converted into dry-air values based on water mole fractions measured by the same instrument. From these, the partial pressures (pCO_2/pCH_4) were calculated assuming 100 % humidity in the equilibrator headspace (water vapour pressure by Weiss and Price, 1980). The pCO_2 was temperature-corrected to account for water warming from the inlet to the equilibrator (Takahashi et al., 1993). CH_4 partial pressure data were converted to concentration (cCH_4) using the solubility constants given in Wiesenburg and Guinasso (1979). All equilibrator data were averaged using a 1 min rolling mean to match the temporal resolution of other Ferrybox parameters.

Despite the fact that we actually recorded mole fractions (xCO_2 and xCH_4), we report our CO_2 data as pCO_2 and CH_4 data as cCH_4, considering that these units are usually reported in studies addressing the respective gases. Accordingly, the atmospheric data were displayed as atmospheric partial pressure for CO_2 or saturation concentration calculated from temperature and salinity for CH_4.

Surface flow-through pCO_2 and cCH_4 data recorded at the monitoring stations were excluded using a speed of the vessel of less than 0.6 kn as the criterion. This was necessary because during profiling and water sampling the sampling device or ship propulsion could bring up sub-surface water, which caused artificial spikes in pCO_2 and cCH_4 signals.

3.4 CTD profiles and upper mixed layer depth

Vertical profiles of temperature, salinity, Chl *a* fluorescence, and dissolved oxygen were recorded at the monitoring stations using the CTD probe (Ocean Seven 320plus; Idronaut s.r.l). Salinity and the density anomaly are shown as absolute salinity ($g\,kg^{-1}$) and sigma-0 ($kg\,m^{-3}$), respectively, and were calculated using the TEOS-10 equation of state (IOC et al., 2010). The depth of the UML was determined from the CTD profiles at the monitoring stations to evaluate whether vertical mixing reached all the way down to the seabed. It was done by comparing the UML depth with the water depth along the ship track adjacent to each station. The UML depth was defined according to Liblik and Lips (2012) as the minimum depth, where $\rho_z - \rho_3 > 0.25\,kg\,m^{-3}$, where ρ_z is the density anomaly at depth z and ρ_3 at a depth of 3 m.

3.5 Air–sea CO_2 and CH_4 flux calculations

Air–sea gas exchange calculations were performed using the FluxEngine toolbox. The FluxEngine toolbox is an open-source software package described in more detail by Shutler et al. (2016) and Holding et al. (2019).

The CO_2 fluxes were calculated using a rapid model approach (Woolf et al., 2016) implemented into the FluxEngine toolbox:

$$F = k\left(\alpha_W pCO_{2_W} - \alpha_A pCO_{2_A}\right), \quad (1)$$

where F ($g\,C\,m^{-2}\,d^{-1}$) denotes the flux across the interface, k the gas transfer velocity, α the solubility of gas in the sub-surface water and the water surface (subscripts W and A, respectively) and pCO_2 partial pressure of CO_2 in the sea surface water and atmosphere (subscripts W and A, respectively).

Methane fluxes were calculated using the same approach as for CO_2 fluxes:

$$F = k\left(cCH_{4_W} - cCH_{4_A}\right), \quad (2)$$

where cCH_4 is concentration of CH_4 in the surface seawater and atmosphere (subscripts W and A, respectively).

In order to accurately describe the fluxes and the carbon budget, it is essential to include relevant processes to the air–sea CO_2 and CH_4 flux parameterization. Nightingale et al. (2000) was used for the gas transfer velocity parameterization for both CO_2 and CH_4 in our study. The sensitivity analysis of the gas transfer velocity in the Baltic Sea (Gutiérrez-Loza et al., 2021) used different parameterizations of the gas transfer velocity to evaluate the effect of other relevant processes in addition to wind speed on the net CO_2 flux at regional and sub-regional scales. In the Estonian sea area, they observed negligible differences in the average net CO_2 flux when using the different gas transfer parameterizations relative to the wind-based parameterization:

$$k = \left(0.222U_{10}^2 + 0.333U_{10}\right)\sqrt{600/Sc}, \quad (3)$$

where U_{10} is the wind speed at 10 m above the sea surface and Sc is the Schmidt number. The Schmidt number parameterization was based on Wanninkhof (2014).

4 Results

4.1 Meteorological conditions

Meteorological conditions in the Baltic Sea area in 2018 were characterized by warmer than long-term average air and sea surface temperatures (Hoy et al., 2020; Humborg et al., 2019). Net solar radiation was above the average seasonal curve from February to September, with the maximum positive deviation in May (Fig. 2). In accordance with the latter, the monthly mean air temperature exceeded the long-term average from April until the end of the year. Except for June, the monthly mean wind speed in the spring and summer of 2018 was lower than the long-term average. All these meteorological parameters predict that the sea surface temperature should have been higher and seasonal vertical stratification

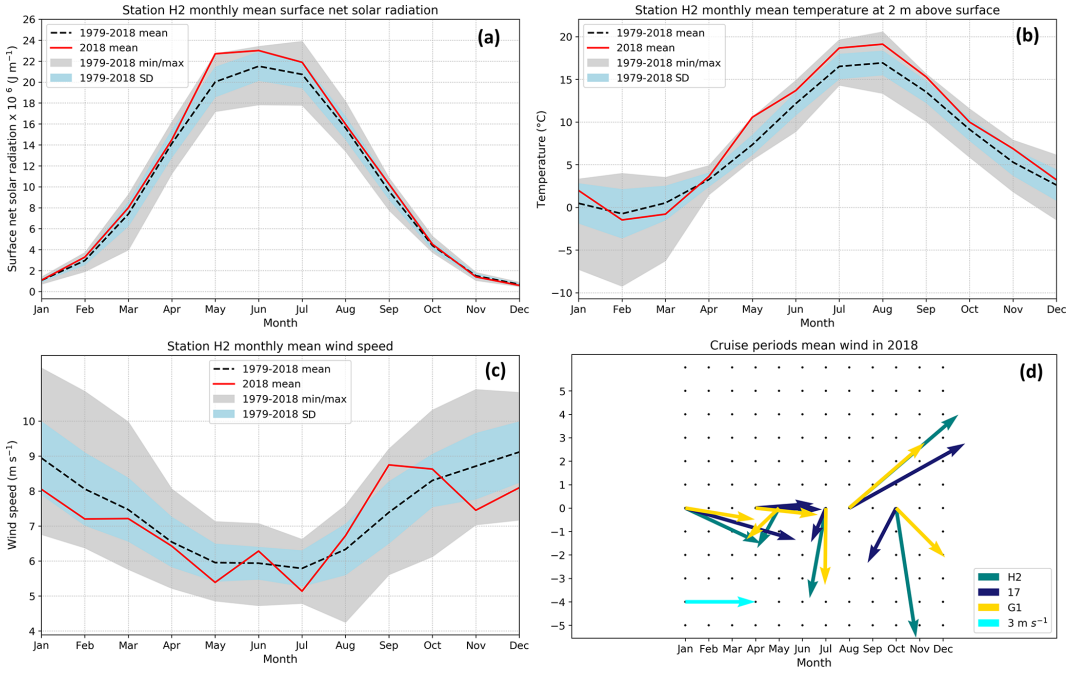

Figure 2. Monthly average **(a)** surface net solar radiation, **(b)** air temperature, and **(c)** wind speed in 2018 (red line) compared with the long-term averages (dashed black line), standard deviations (blue area), and minimum–maximum values (grey area) in the NBP (station H2) for the period 1979–2018. **(d)** Cruise period average wind vectors in the NBP (H2, green), GoF (17, blue), and GoR (G1, yellow). See Fig. 1 for the locations of stations and model grid points for data extraction.

stronger than on average due to the increased positive buoyancy flux and weak wind-induced mixing.

The winds from west and south-west prevailed during and before the cruises in January, April, and August (Fig. 2), which is in accordance with the general airflow in the study area. During the cruises in July and October, the wind direction was generally from the north or north-east, while weak winds from the same direction prevailed in May–June. Note that the northerly and north-easterly winds in July and October were favourable for the upwelling development along the south-western coast of the Gulf of Finland and the eastern coasts in the Northern Baltic Proper.

The variability in wind speed and direction between the three basins and within the cruise periods is presented by the wind roses (see Fig. 3, where wind roses for three cruise periods with larger wind forcing and spatial variability are presented). The winds were mostly from one direction during the cruise in August, and a wider spread was characteristic for the cruise periods in July and October. In July, mostly two directions prevailed: easterly winds, which could cause upwelling events along the entire southern coast of the Gulf of Finland, and north-westerly winds, which are upwelling favourable for the eastern coasts of the NBP. In October, the spread of directions was the largest, but the strongest winds with speeds exceeding $15\,\mathrm{m\,s^{-1}}$ in the GoF and NBP were from the north-east. In the GoR, wind speeds were generally lower than in the other two basins.

4.2 Spatial variability

Surface water pCO_2 and cCH_4 distributions along the R/V track show larger spatial variability in the GoR and GoF than in the NBP for all six cruises (Figs. 4–9). Although the general seasonal pCO_2 course is evident, pCO_2 locally exceeded the atmospheric equilibrium level also during the cruises in April, May, and August. The latter is mostly valid for the GoR, but it is also valid for the GoF in August. cCH_4 was oversaturated in the surface layer during the whole study period, with prominent local peaks of cCH_4 in the GoR and GoF.

In January (Fig. 4), surface water pCO_2 along the cruise track (Fig. 4c) did not show remarkable regional differences. Values fluctuated within the range of 425–550 µatm and were oversaturated in all monitored areas. In almost all areas, the water column was well mixed down to the seabed or permanent halocline. Note that, in contrast to the other cruises, the vessel did not visit mouth areas of the rivers (neither in the GoR nor in the GoF), and cCH_4 was not measured in January.

The cruise in April (Fig. 5) mapped pCO_2 and cCH_4 distributions in the period of the onset of seasonal stratification and spring bloom in different development phases. The surface water pCO_2 (Fig. 5c) was mostly below the atmospheric partial pressure but reached equilibrium with the atmosphere in the western and central GoR. Low Chl *a* and oxygen concentrations indicate that the spring bloom was still in its ini-

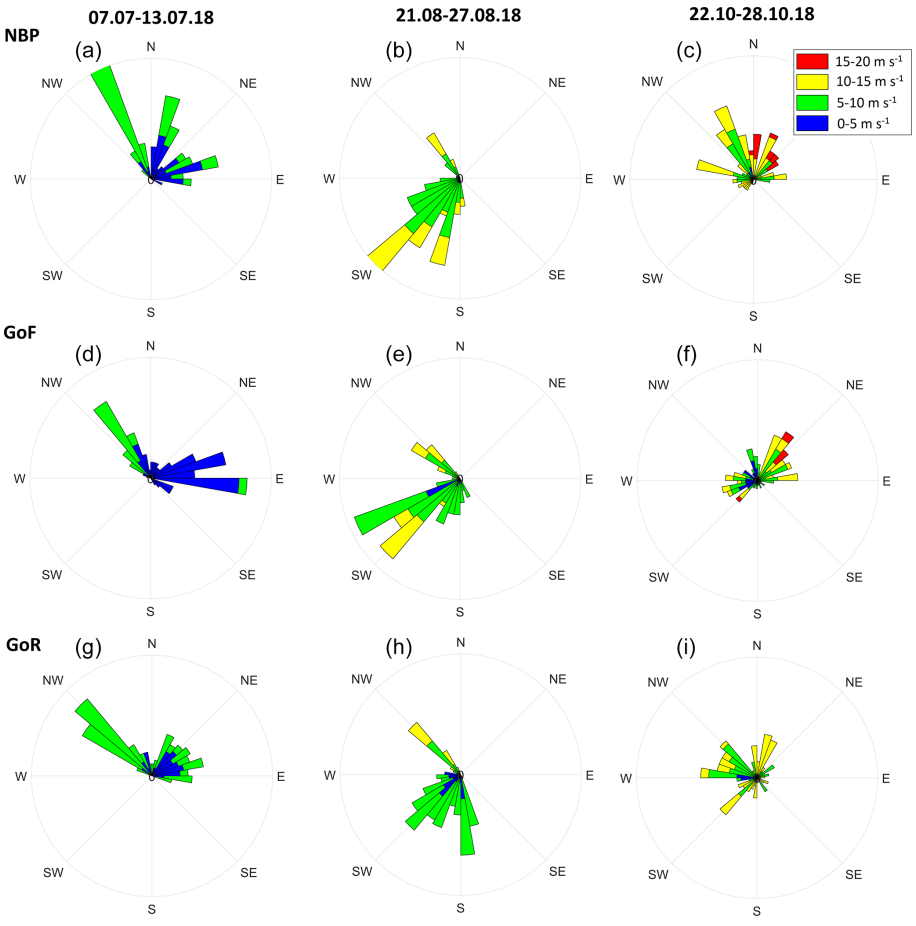

Figure 3. Cruise period wind roses in July **(a, d, g)**, August **(b, e, h)**, and October **(c, f, i)** 2018 in the NBP **(a, b, c)**, GoF **(d, e, f)**, and GoR **(g, h, i)** based on the hourly ERA5 data extracted from a grid point close to the monitoring stations H2, 17, and G1, respectively (see locations in Fig. 1). The radial axis maximum is 30 (out of 168).

tial phase in this area (Fig. 5d). In addition, the water column was mixed almost down to the seabed in this sea area. The pCO_2 values were clearly lower in the eastern part of the open GoR, the shallow Pärnu Bay, and the Väinameri Sea. These pCO_2 minima (down to 60 µatm) were associated with increased temperature and the highest Chl *a* and oxygen concentrations in these areas, while the influence of the Pärnu River was visible via a local peak in the pCO_2 (up to 397 µatm).

From the western GoF towards the central GoF, a Chl *a* increase from < 9 to 15 mg m^{-3} was accompanied by slightly higher oxygen and lower pCO_2 values (about 130 µatm). Although high Chl *a* concentrations up to 16 mg m^{-3} were mapped along the south-eastern coast of the GoF, pCO_2 values in this area remained on a higher level (around 250 µatm) than in other regions with a similar surface layer Chl *a* content. Note that the water column along the coast was well mixed down to the seabed, except close to the Narva River mouth. Elevated cCH_4 was measured, similar to the pCO_2 distribution, in the western and central GoR (27–37 nmol L^{-1}) and in Pärnu Bay close to the mouth of the Pärnu River (40 nmol L^{-1}). Elevated cCH_4 was also measured along the south-western coast of the GoF (26 nmol L^{-1}; marked as SW GoF in Fig. 5e), where the water column was mixed down to the seabed, and close to the mouth of the Narva River (up to 30 nmol L^{-1}). The direct influence of the Pärnu and Narva rivers was expressed by the cCH_4 peaks.

The cruise at the end of May and beginning of June (Fig. 6) coincided with the phytoplankton summer minimum, while the water column was characterized by unusually high sea surface temperatures (13–18 °C; Fig. 6b) and a shallow upper mixed layer (Fig. 6a, on average < 6 m in the GoR and 8 m in the central GoF). The pCO_2 values had decreased to the minimum along most of the ship track, varying mostly between 50 and 100 µatm, while moderately higher (reaching 200 µatm) than background pCO_2 values were registered in the NBP–GoR transition area, the Irbe Strait. CO_2 oversaturation was locally recorded in the shallowest areas of the GoR – Pärnu Bay and the Väinameri Sea. In Narva Bay,

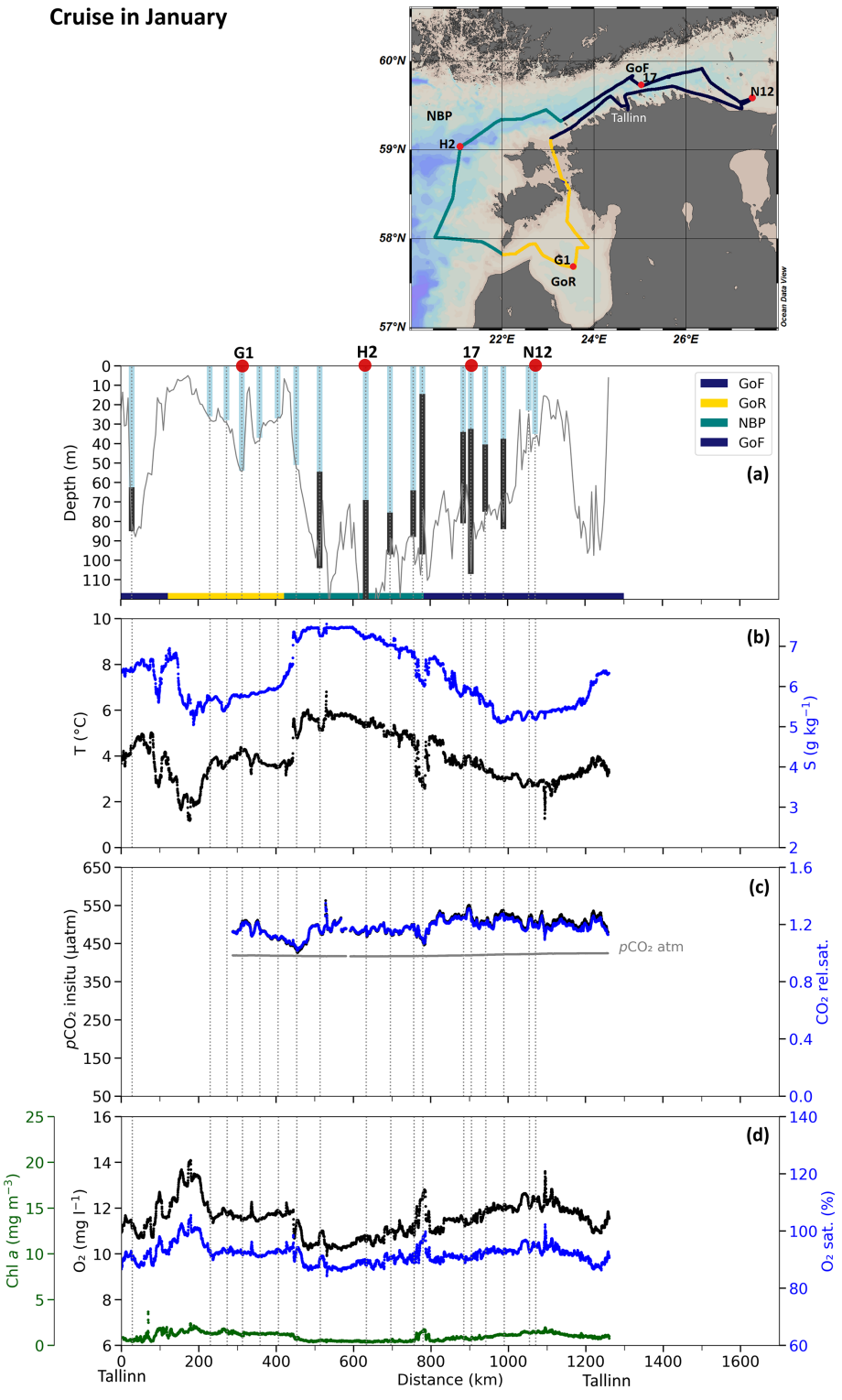

Figure 4. January monitoring cruise (8–12 January). The trajectory is shown on the map, and in panel **(a)** the UML depth (light blue bars) and the water column extent below the UML (dark blue bars) are shown; vertical dashed grey lines indicate the locations of monitoring stations, while the locations of the most characteristic stations of the sub-basins are denoted with red dots. **(b)** Spatial variability of temperature (left *y* axis) and salinity (right *y* axis); **(c)** CO_2 partial pressure (left *y* axis) and relative saturation (right *y* axis); and **(d)** Chl *a* (left *y* axis), dissolved oxygen concentration (left *y* axis), and saturation (right *y* axis) are also shown. The *x* axis denotes the distance (in km) from the start of the monitoring cruise (Tallinn). The map was generated using Ocean Data View (Reiner Schlitzer, Ocean Data View, https://odv.awi.de/, last access: 14 February 2023, 2022).

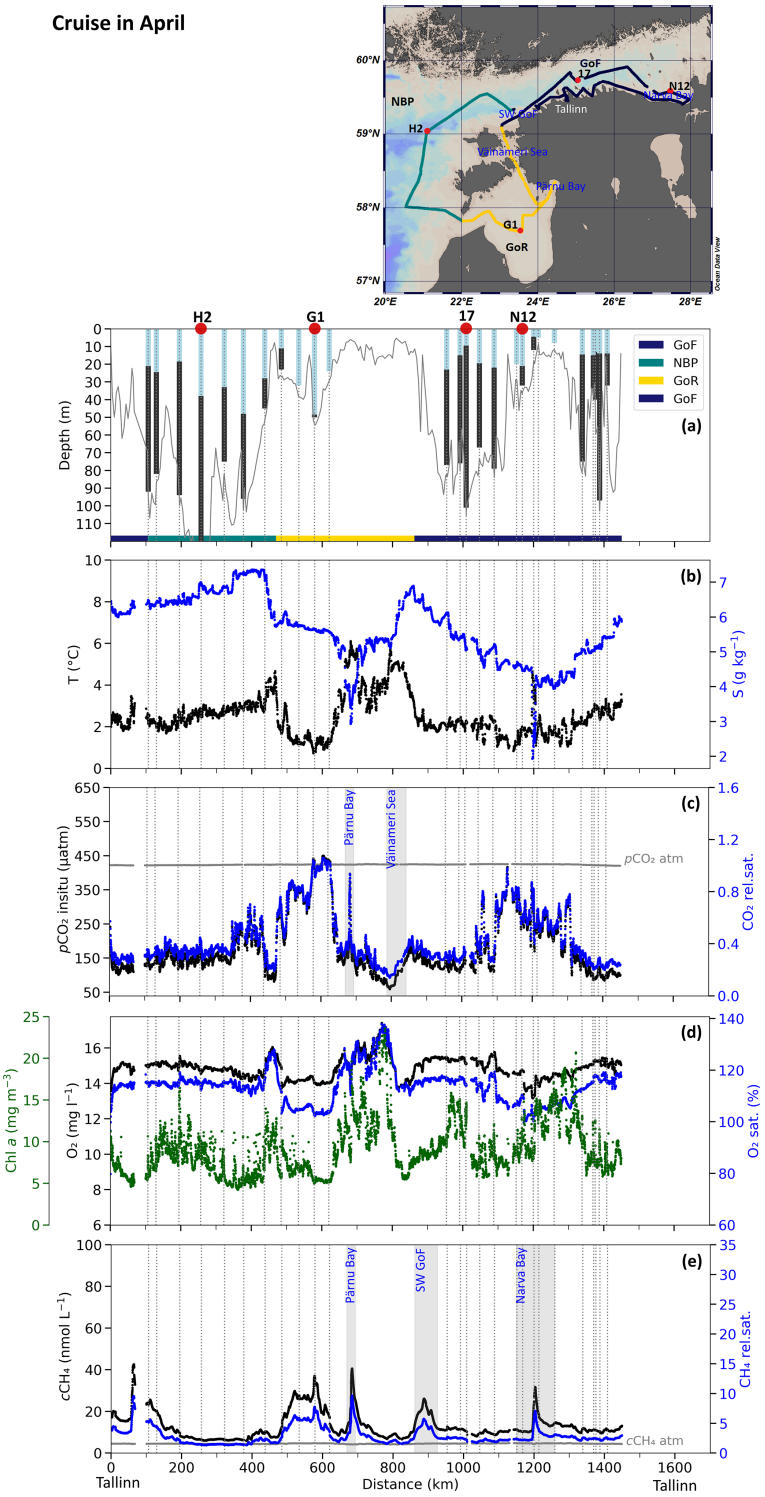

Figure 5. April monitoring cruise (16–20 April). The trajectory is shown on the map, and in panel **(a)** the UML depth (light blue bars) and the water column extent below the UML (dark blue bars) are shown; vertical dashed grey lines indicate the locations of monitoring stations, while the locations of the most characteristic stations of the sub-basins are denoted with red dots. **(b)** Spatial variability of temperature (left *y* axis) and salinity (right *y* axis); **(c)** CO_2 partial pressure (left *y* axis) and relative saturation (right *y* axis); **(d)** Chl *a* (left *y* axis), dissolved oxygen concentration (left *y* axis), and saturation (right *y* axis); and **(e)** CH_4 concentration (left *y* axis) and relative saturation (right *y* axis) are also shown. The *x* axis denotes the distance (in km) from the start of the monitoring cruise (Tallinn). The map was generated using Ocean Data View (Reiner Schlitzer, Ocean Data View, https://odv.awi.de/, last access: 14 February 2023, 2022).

no distinct Narva River impact was registered. Local cCH_4 maxima were observed in the shallow bays of the southern and south-western GoF ($> 80\,nmol\,L^{-1}$) and in the Irbe Strait close to the Kolka Peninsula ($> 35\,nmol\,L^{-1}$). Only slightly higher than background cCH_4 values were measured in the southern GoR close to the mouths of the largest rivers – the Daugava and Lielupe. In contrast, an extensive peak in cCH_4 was registered in the shallow Pärnu Bay close to the Pärnu River (maximum measured concentration was $232\,nmol\,L^{-1}$). Local maxima in the shallow Väinameri Sea increased to notable peaks along the south-western coast of the GoF. Local maxima of $33\,nmol\,L^{-1}$ in Narva Bay were likely due to the influence of the Narva River.

In mid-July (Fig. 7), the surface waters were undersaturated in CO_2 along the entire ship track (Fig. 7c; note that the vessel did not visit the mouth areas of the Pärnu and Narva rivers). The UML has slightly deepened in the GoR (8 m) but was the shallowest in the offshore GoF (< 7 m). Higher than $5\,mg\,m^{-3}$ Chl *a* concentrations were observed in the offshore areas of NBP, the north-eastern GoR, and the central GoF, probably due to the development of the summer bloom. Elevated pCO_2 values were recorded in parts of the NBP offshore areas (330 µatm) and the coastal sea area in the Irbe Strait (310 µatm) and the Väinameri Sea (355 µatm). Local maxima of cCH_4 up to $43\,nmol\,L^{-1}$ were observed in the shallow bays of the southern and south-western GoF, including the transition area into the GoF. In comparison with the cruise at the end of May, in July a relatively low cCH_4 peak ($14\,nmol\,L^{-1}$) was observed in the Irbe Strait, and the influence of large rivers in the southern GoR was almost not detectable.

In August (Fig. 8), CO_2 varied around the saturation level. The surface waters were undersaturated in CO_2 in most areas of the GoF except Narva Bay, where the water column was well-mixed down to the seabed; oversaturated in the Väinameri Sea and Pärnu Bay; and undersaturated in the NBP (Fig. 8c). These higher pCO_2 values were characteristic for the shallow areas and could be only partly related to the river discharge (as in Narva Bay and Pärnu Bay). A distinct local maximum in pCO_2 of 460 µatm was related to the salinity front in the Irbe Strait, as also observed earlier. Local cCH_4 maxima were observed in the shallow bays of the southern and south-western GoF and along the south-eastern coast of Narva Bay. Locally, well-pronounced cCH_4 peaks with a maximum concentration of $177\,nmol\,L^{-1}$ were also observed in the Väinameri Sea and Pärnu Bay. The increase in cCH_4 in the Irbe Strait ($38\,nmol\,L^{-1}$) was comparable with the cCH_4 peak at the end of May cruise.

In October (Fig. 9), surface waters were oversaturated in CO_2 almost along the entire ship track (Fig. 9c). Like during the August cruise, pCO_2 values were lower in the NBP (varying between 400 and 480 µatm) than in the GoF and GoR (varying up to 600 µatm). In contrast to the summer cruises, higher pCO_2 values were characteristic for the offshore areas in the GoR, and lower values were present in the shallow coastal sea areas – Pärnu Bay and the Väinameri Sea. The pCO_2 values exceeding 1200 µatm were registered in connection to an upwelling event in the SW GoF caused by the strong north-westerly winds before and during the cruise. Peaks in cCH_4 up to $80\,nmol\,L^{-1}$ were registered in the shallow bays along the southern coast of the GoF. In the Irbe Strait, cCH_4 increased up to $15\,nmol\,L^{-1}$ in October. A clear cCH_4 peak of $62\,nmol\,L^{-1}$ was detected in Pärnu Bay, probably influenced by the Pärnu River discharge. Local maxima in the Väinameri Sea increased to an extensive broad peak ($69\,nmol\,L^{-1}$) in the upwelling waters in the SW GoF.

4.3 Seasonal variability

Seasonal variability of pCO_2 in 2018 (Fig. 10d) follows the general seasonal course in all analysed sub-basins (Table 1), with oversaturation in autumn–winter (average relative CO_2 saturation 1.2) and undersaturation in spring–summer (average relative CO_2 saturation 0.5). The pCO_2 decrease in spring coincides with the highest Chl *a* and dissolved oxygen concentrations in April. Based on decreased Chl *a* concentrations from mid-April to the end of May (Fig. 10e; Table 1), the early summer minimum of phytoplankton biomass was evident. It is also at the end of May to early June when the pCO_2 seasonal minimum in all sub-basins appeared (Table 1). During midsummer, relatively high Chl *a* concentrations were recorded (Fig. 10e; Table 1), while dissolved oxygen concentrations stayed moderately oversaturated. The pCO_2 values increased from July on, reaching oversaturation almost everywhere along the cruise track by the October cruise. No second pCO_2 minimum during summer or relative maximum between the two usually expected minima in spring and late summer was detected.

For the evaluation of the seasonal course of surface water methane concentrations, cCH_4 median values were analysed (Fig. 10h and Table 1). In all three sub-basins, the highest median concentrations of $13.7\,nmol\,L^{-1}$ in the GoR, $11.5\,nmol\,L^{-1}$ in the GoF, and $7.6\,nmol\,L^{-1}$ in the NBP were determined in April (note we do not have winter data), after which the concentrations started to decrease. The minimum level was reached in the GoF and GoR in July (median concentrations were 7.9 and $4.5\,nmol\,L^{-1}$, respectively) and in the NBP in August ($3.9\,nmol\,L^{-1}$). It was followed by an increase in concentrations by October, but the values did not yet reach the levels observed in April.

Although high cCH_4 values represent only a small part of acquired data, it is worthwhile to mark some seasonal changes in variability. The highest cCH_4 variations were observed in May, August, and October in the GoF and in April, May, and August in the GoR. It shows that although the average seasonal course in the GoF and GoR was similar to the NBP, regions existed in the GoF and GoR with locally high methane concentrations (extremes exceeding $100\,nmol\,L^{-1}$).

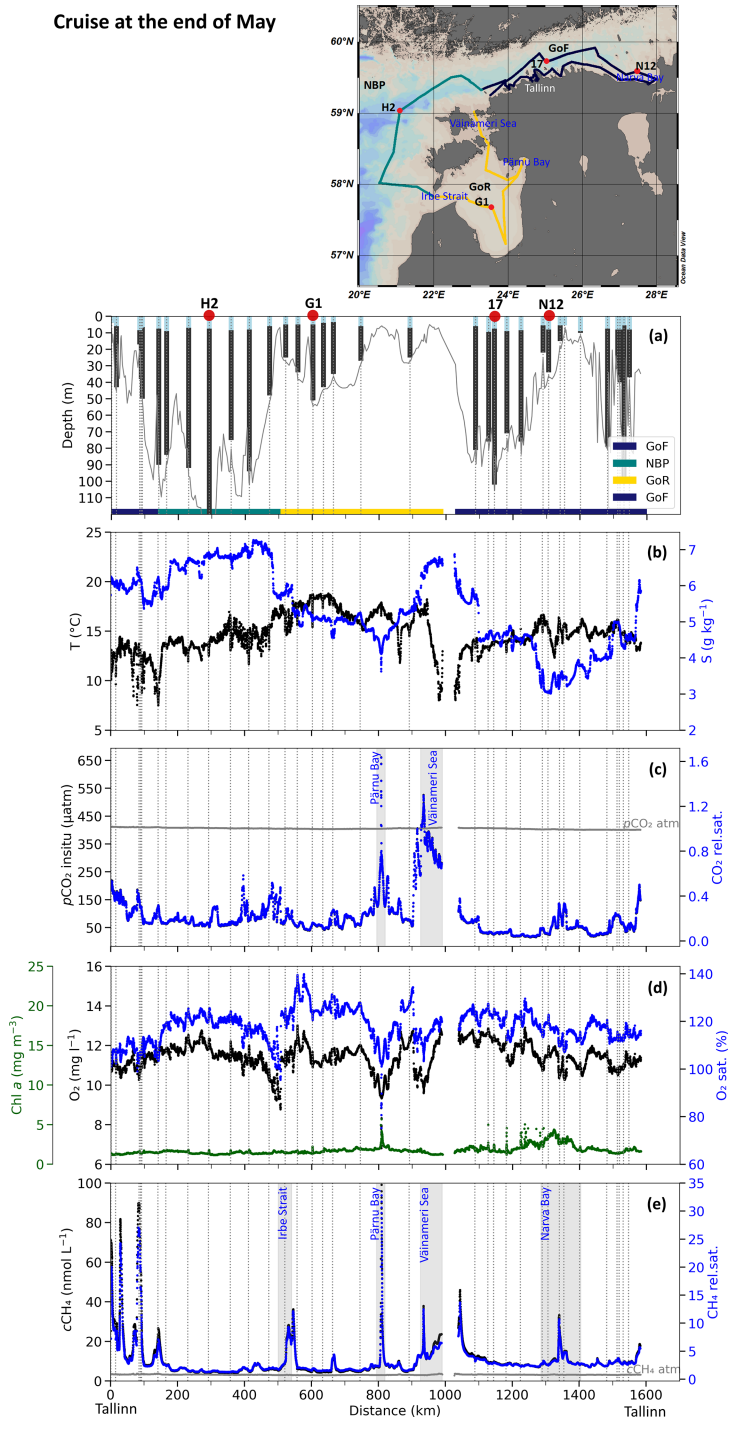

Figure 6. End of May monitoring cruise (28 May–2 June). The trajectory is shown on the map, and in panel **(a)** the UML depth (light blue bars) and the water column extent below the UML (dark blue bars) are shown; vertical dashed grey lines indicate the locations of monitoring stations, while the locations of the most characteristic stations of the sub-basins are denoted with red dots. **(b)** Spatial variability of temperature (left *y* axis) and salinity (right *y* axis); **(c)** CO_2 partial pressure (left *y* axis) and relative saturation (right *y* axis); **(d)** Chl *a* (left *y* axis), dissolved oxygen concentration (left *y* axis), and saturation (right *y* axis); and **(e)** CH_4 concentration (left *y* axis) and relative saturation (right *y* axis) are also shown. The *x* axis denotes the distance (in km) from the start of the monitoring cruise (Tallinn). In May, the cCH_4 signal in the river estuaries was extreme in comparison with the rest of the data, and this signal was cut here to 100 nmol L^{-1} to properly display the structure within low-concentration areas. Note the different scale for temperature in comparison with January and April (Fig. 4 and 5, respectively). The map was generated using Ocean Data View (Reiner Schlitzer, Ocean Data View, https://odv.awi.de/, last access: 14 February 2023, 2022).

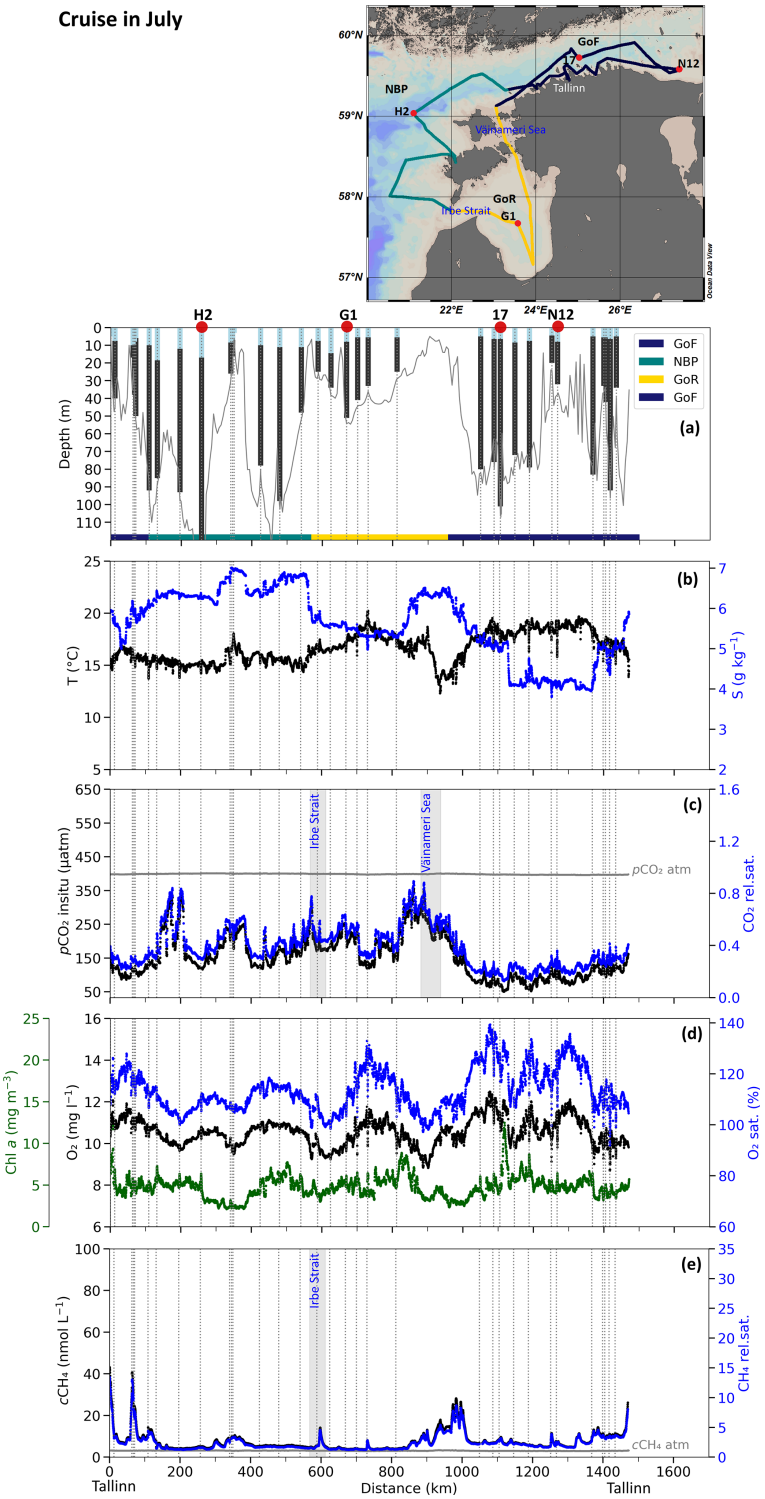

Figure 7. July monitoring cruise (9–13 July). The trajectory is shown on the map, and in panel **(a)** the UML depth (light blue bars) and the water column extent below the UML (dark blue bars) are shown; vertical dashed grey lines indicate the locations of monitoring stations, while the locations of the most characteristic stations of the sub-basins are denoted with red dots. **(b)** Spatial variability of temperature (left *y* axis) and salinity (right *y* axis); **(c)** CO_2 partial pressure (left *y* axis) and relative saturation (right *y* axis); **(d)** Chl *a* (left *y* axis), dissolved oxygen concentration (left *y* axis), and saturation (right *y* axis); and **(e)** CH_4 concentration (left *y* axis) and relative saturation (right *y* axis) are also shown. The *x* axis denotes the distance (in km) from the start of the monitoring cruise (Tallinn). The map was generated using Ocean Data View (Reiner Schlitzer, Ocean Data View, https://odv.awi.de/, last access: 14 February 2023, 2022).

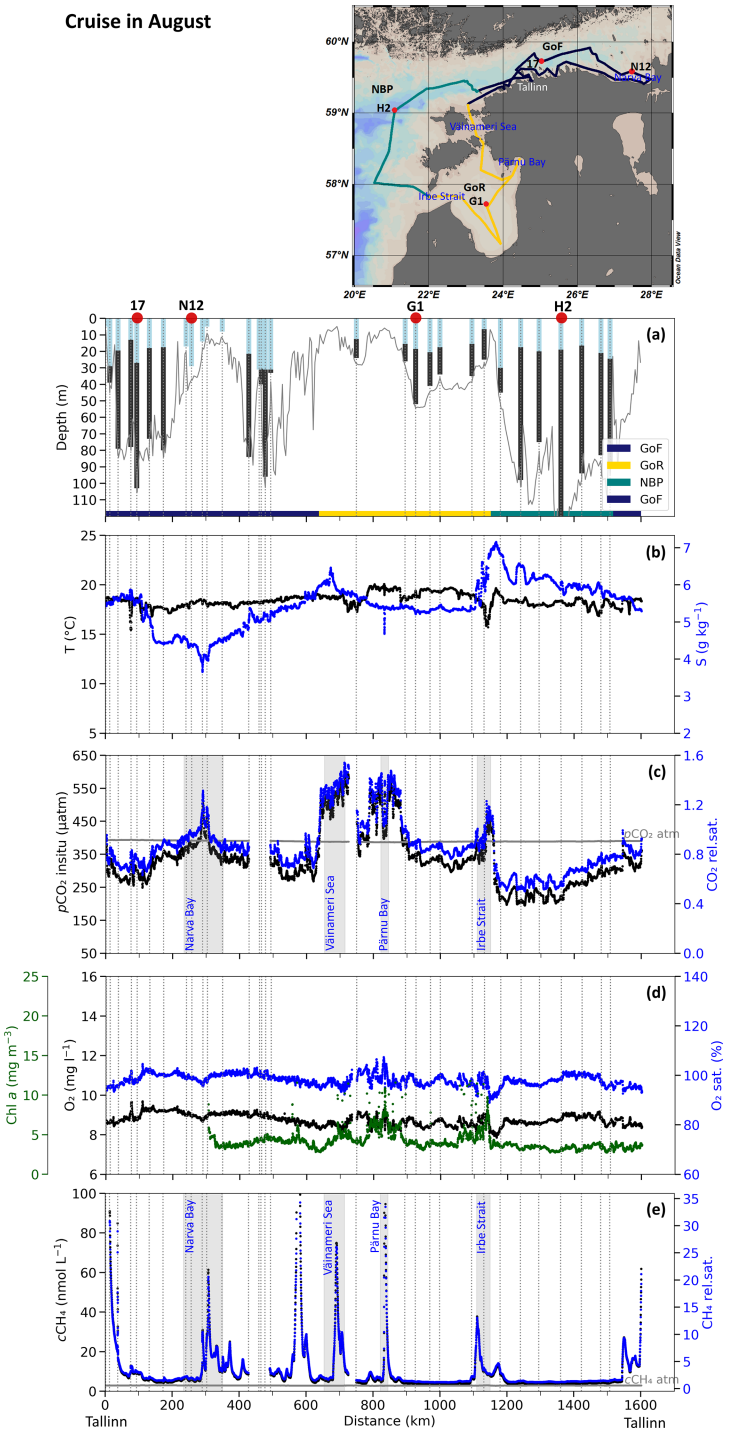

Figure 8. August monitoring cruise (22–27 August). The trajectory is shown on the map, and in panel **(a)** the UML depth (light blue bars) and the water column extent below the UML (dark blue bars) are shown; vertical dashed grey lines indicate the locations of monitoring stations, while the locations of the most characteristic stations of the sub-basins are denoted with red dots. **(b)** Spatial variability of temperature (left *y* axis) and salinity (right *y* axis); **(c)** CO_2 partial pressure (left *y* axis) and relative saturation (right *y* axis); **(d)** Chl *a* (left *y* axis), dissolved oxygen concentration (left *y* axis), and saturation (right *y* axis); and **(e)** CH_4 concentration (left *y* axis) and relative saturation (right *y* axis) are also shown. The *x* axis denotes the distance (in km) from the start of the monitoring cruise (Tallinn). In August, cCH_4 signals in the river estuaries and coastal areas were extreme in comparison with the rest of the data, and these signals were cut here to 100 nmol L^{-1} to properly display the structure within low-concentration areas. The map was generated using Ocean Data View (Reiner Schlitzer, Ocean Data View, https://odv.awi.de/, last access: 14 February 2023, 2022).

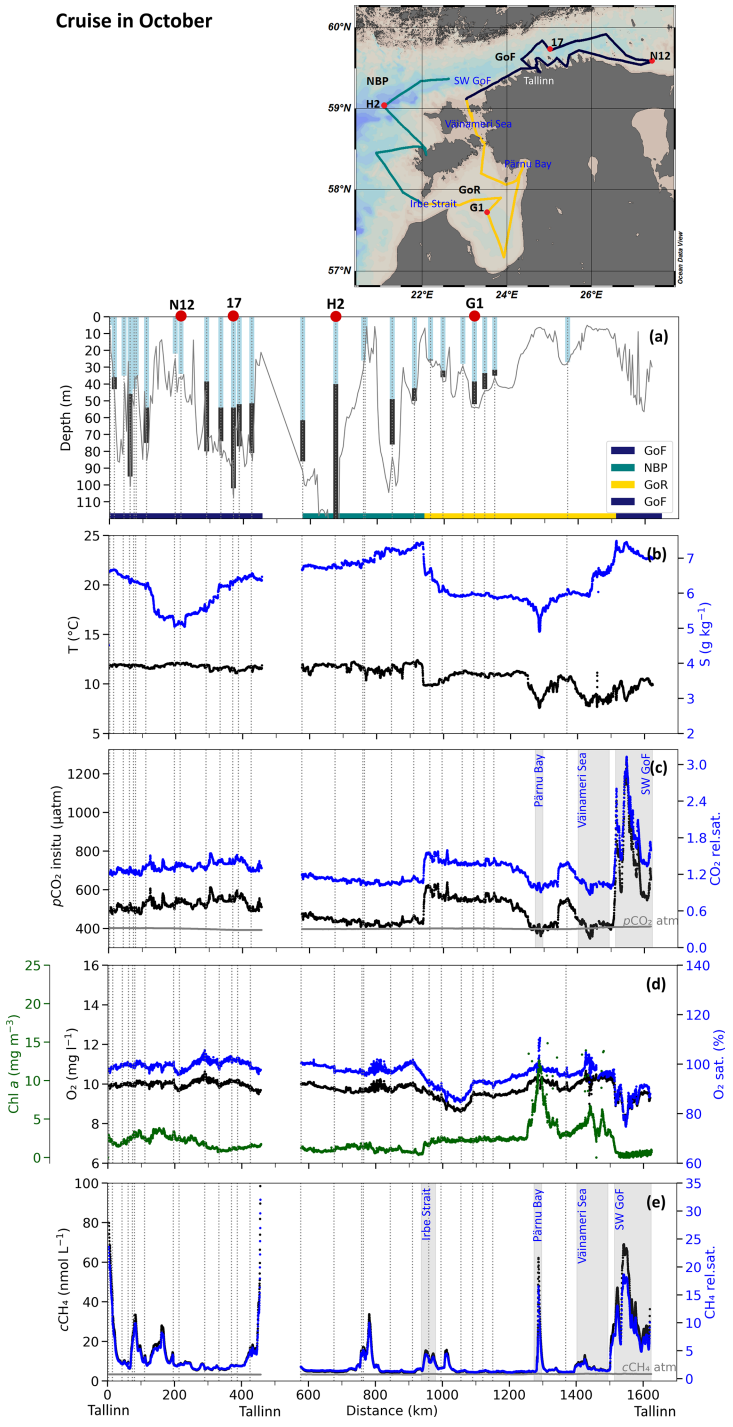

Figure 9. October monitoring cruise (22–28 October). The trajectory is shown on the map, and in panel **(a)** the UML depth (light blue bars) and the water column extent below the UML (dark blue bars) are shown; vertical dashed grey lines indicate the locations of monitoring stations, while the locations of the most characteristic stations of the sub-basins are denoted with red dots. **(b)** Spatial variability of temperature (left *y* axis) and salinity (right *y* axis); **(c)** CO_2 partial pressure (left *y* axis) and relative saturation (right *y* axis); **(d)** Chl *a* (left *y* axis), dissolved oxygen concentration (left *y* axis), and saturation (right *y* axis); and **(e)** CH_4 concentration (left *y* axis) and relative saturation (right *y* axis) are also shown. The *x* axis denotes the distance (in km) from the start of the monitoring cruise (Tallinn). In October, cCH_4 signal in the coastal areas was extreme in comparison with the rest of the data, and this signal was cut here to 100 nmol L^{-1} to properly display the structure within low-concentration areas. Note the different scales for CO_2 partial pressure and relative saturation in comparison with the rest of the cruises. The map was generated using Ocean Data View (Reiner Schlitzer, Ocean Data View, https://odv.awi.de/, last access: 14 February 2023, 2022).

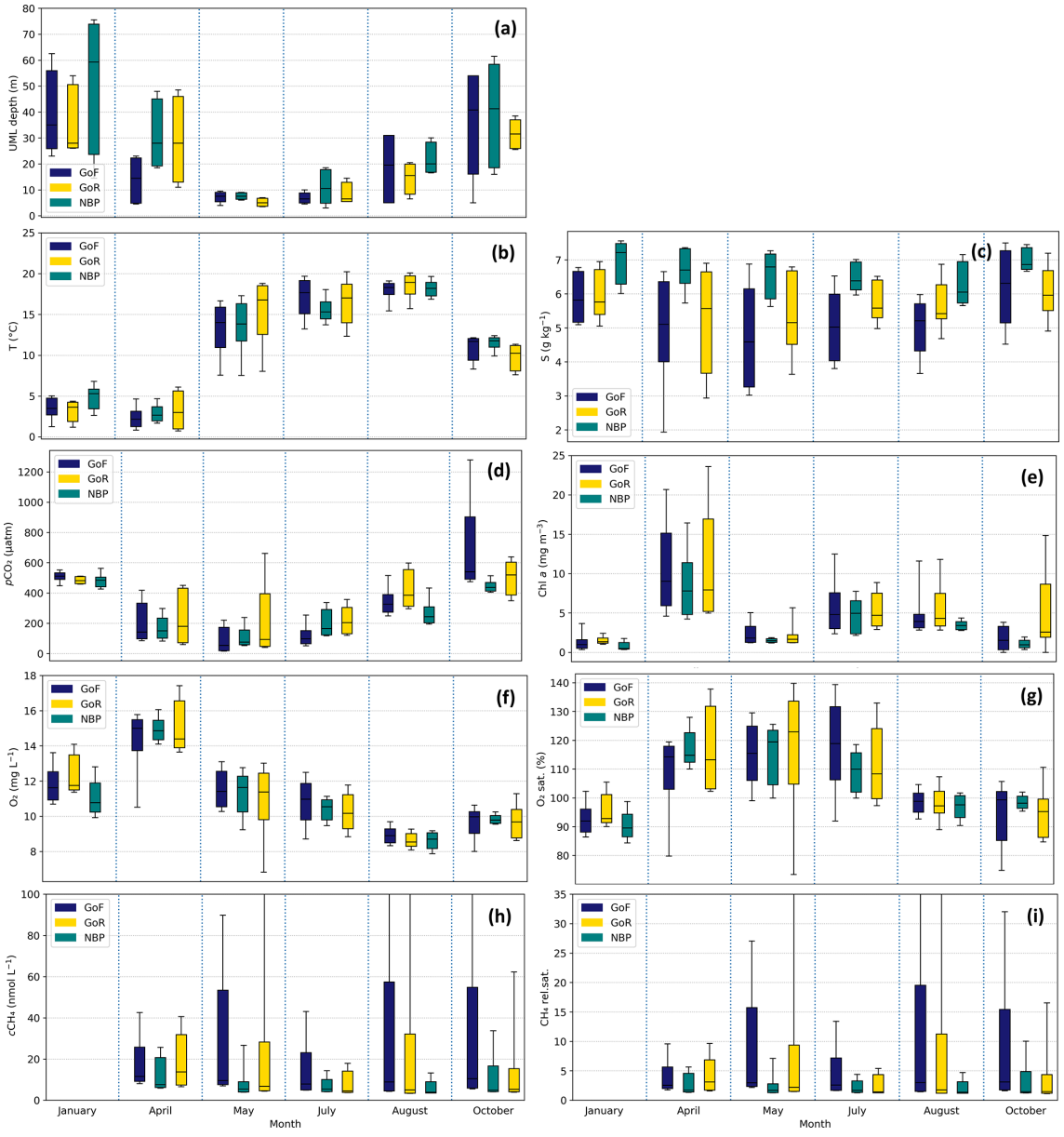

Figure 10. Median and 5th and 95th percentile values of **(a)** UML depth, **(b)** temperature, **(c)** salinity, **(d)** CO_2 partial pressure, **(e)** Chl *a*, **(f)** dissolved oxygen, **(g)** oxygen saturation, **(h)** CH_4 concentration, and **(i)** CH_4 relative saturation. Whiskers denote minimum and maximum values. In the May, August, and October cruises, cCH_4 signals in the river estuaries and coastal areas were extreme in comparison with the rest of the data, and these signals are not seen on the plot (y-axis maximum is 100 nmol L^{-1} to properly display the pattern in low-concentration areas).

4.4 Estimates of the air–sea CO_2 and CH_4 fluxes

The air–sea CO_2 and CH_4 fluxes calculated for every research cruise were seasonally averaged so that winter is characterized by the cruise in January, spring by the cruises in April and May, summer by the cruises in July and August, and autumn by the cruise in October (Tables 2 and 3; Fig. 11).

The CO_2 flux estimates (Table 2) show that the Estonian sea area was a source of atmospheric CO_2 (positive flux) during winter and autumn and a sink (negative flux) during spring and summer 2018. What stands out is that the standard deviations are of the same order of magnitude as the estimated average fluxes. The observed spatial variability was larger in the GoR and GoF than in the NBP (Figs. 4–9). The annual mean flux (estimated as an arithmetic average of the four seasonal flux estimates) was $-0.06\,g\,C\,m^{-2}\,d^{-1}$ in the NBP, $-0.02\,g\,C\,m^{-2}\,d^{-1}$ in the GoF, and $-0.005\,g\,C\,m^{-2}\,d^{-1}$ in the GoR.

Table 1. Median and mean (value before and after the slash, respectively) values of UML depth, temperature (T), salinity (S), CO_2 partial pressure (pCO_2), Chl a, dissolved oxygen (O_2), oxygen saturation (O_2 sat.), CH_4 concentration (cCH_4), and CH_4 relative saturation (CH_4 rel.) for the Estonian sea area sub-basins in 2018.

		UML (m)	T (°C)	S ($g\,kg^{-1}$)	pCO_2 (µatm)	Chl a ($mg\,m^{-3}$)	O_2 ($mg\,L^{-1}$)	O_2 sat. (%)	cCH_4 ($nmol\,L^{-1}$)	CH_4 rel. sat. (%)
GoF	January	35/38	3.5/3.5	5.8/5.9	511/511	1.0/1.0	11.6/11.7	92/92	–	–
	April	15/15	2.2/2.2	5.1/5.1	141/178	9.0/9.7	15.0/14.9	114/112	11.5/13.8	2.5/3.0
	May	8/7	14.0/13.9	4.6/4.7	53/70	1.8/2.0	11.4/11.5	115/116	9.5/15.4	3.0/4.7
	July	7/7	17.7/17.4	5.0/4.9	97/102	4.8/5.0	11.0/10.9	119/119	7.9/9.9	2.6/3.2
	August	20/20	18.3/18.2	5.2/5.1	326/327	3.9/4.0	8.9/8.9	99/99	8.8/17.7	3.0/6.0
	October	41/40	11.7/11.4	6.3/6.2	540/580	1.5/1.7	10.0/9.8	99/97	10.5/17.9	3.1/5.2
NBP	January	59/55	5.3/5.1	7.2/7.1	484/480	0.5/0.6	10.8/10.8	90/90	–	–
	April	28/30	2.7/2.7	6.7/6.7	149/158	7.8/7.8	14.9/14.9	115/115	7.6/9.3	1.7/2.1
	May	8/8	13.8/13.9	6.8/6.7	75/86	1.5/1.5	11.6/11.5	119/118	5.4/6.1	1.7/1.9
	July	11/11	15.3/15.4	6.4/6.5	165/179	5.0/4.6	10.5/10.4	110/110	5.3/6.0	1.7/1.9
	August	20/21	18.2/18.2	6.1/6.1	243/250	3.4/3.4	8.7/8.7	98/98	3.9/4.5	1.3/1.5
	October	41/39	11.8/11.7	6.9/7.0	436/438	1.0/1.0	9.8/9.8	98/98	4.9/6.7	1.5/2.0
GoR	January	28/34	3.6/3.4	5.8/5.8	482/483	1.3/1.4	11.7/12.1	93/94	–	–
	April	28/29	3.0/3.0	5.6/5.4	180/227	7.9/9.2	14.4/14.8	113/115	13.7/16.6	3.1/3.7
	May	5/5	16.8/16.4	5.2/5.3	93/148	1.7/1.7	11.4/11.3	123/121	6.7/12.4	2.2/4.0
	July	7/8	17.0/17.0	5.6/5.7	204/210	4.7/4.9	10.2/10.2	108/110	4.5/6.1	1.4/2.0
	August	16/15	18.9/18.9	5.4/5.6	385/413	4.3/4.8	8.5/8.6	97/98	5.0/10.2	1.8/3.6
	October	32/31	10.2/10.0	6.0/6.0	519/495	2.6/3.5	9.7/9.7	95/94	5.3/7.3	1.5/2.0

Table 2. Seasonal and annual CO_2 flux estimates with standard deviations for the Estonian sub-basins and sea area in 2018.

	Seasonal median/mean CO_2 fluxes ($g\,C\,m^{-2}\,d^{-1}$; ± standard deviation)			
	GoF	NBP	GoR	Estonian sea area
Winter	0.06/0.07 (±0.04)	0.02/0.02 (±0.02)	0.08/0.07 (±0.05)	0.04/0.05 (±0.04)
Spring	−0.30/−0.36 (±0.23)	−0.14/−0.13 (±0.09)	−0.22/−0.21 (±0.13)	−0.21/−0.26 (±0.20)
Summer	−0.11/−0.11 (±0.06)	−0.16/−0.17 (±0.08)	−0.04/−0.02 (±0.13)	−0.10/−0.10 (±0.11)
Autumn	0.29/0.32 (±0.20)	0.04/0.04 (±0.03)	0.13/0.14 (±0.14)	0.16/0.19 (±0.19)
Annual mean	−0.02	−0.06	−0.005	−0.03

The CH_4 flux estimates (Table 3) show that the Estonian sea area was a source of atmospheric CH_4 during spring, summer, and autumn (no data for winter). Note that the standard deviations of flux estimates exceeded the resulting average fluxes during summer and autumn. As with CO_2 fluxes, the spatial variability of observed CH_4 fluxes was larger in the GoR and GoF than in the NBP (Fig. 11).

5 Discussion

The first extensive trace gases study was conducted to describe spatial patterns and seasonal dynamics of CO_2 and CH_4 in the north-eastern Baltic Sea area. The main focus was on the southern Gulf of Finland and the Gulf of Riga, as earlier studies addressed measurements from the Baltic Proper and the western Gulf of Finland (e.g. Schneider et al., 2014; Schneider and Müller, 2018; Gülzow et al., 2013).

5.1 Patterns of variability in the southern GoF and GoR

5.1.1 pCO_2 distribution patterns

Cruises of R/V *Salme* covered both the offshore and the coastal areas in the GoF and GoR, with the most prominent local pCO_2 peaks in the shallow coastal sea areas. These local maxima were mostly linked to river bulges, coastal upwelling events, fronts, and vertical mixing reaching the seabed but also to phytoplankton distribution patterns influenced by meteorological and hydrographic conditions.

Rivers are the major carbon source, including dissolved inorganic carbon for the coastal ocean (Dai et al., 2022) and the Baltic Sea (Kuliński and Pempkowiak, 2011). In the GoF, the largest freshwater source along the R/V track was the Narva River (Stålnacke et al., 1999). Its influence, identified

Table 3. Seasonal CH_4 flux estimates with standard deviations for the Estonian sub-basins and sea area in 2018.

	Seasonal median/mean CH_4 fluxes (mg C m^{-2} d^{-1}; ± standard deviation)			
	GoF	NBP	GoR	Estonian sea area
Winter	–	–	–	–
Spring	0.20/0.24 (±0.17)	0.03/0.05 (±0.06)	0.12/0.26 (±0.31)	0.14/0.20 (±0.22)
Summer	0.14/0.43 (±0.99)	0.05/0.06 (±0.07)	0.04/0.18 (±0.46)	0.07/0.25 (±0.71)
Autumn	0.37/0.74 (±0.77)	0.07/0.10 (±0.12)	0.07/0.21 (±0.29)	0.18/0.39 (±0.59)

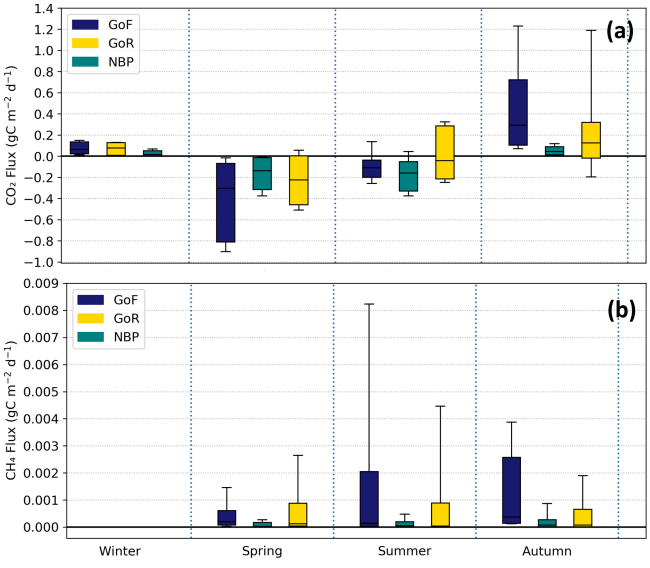

Figure 11. Seasonal median air–sea **(a)** CO_2 and **(b)** CH_4 flux estimates in the three analysed sub-basins of the north-eastern Baltic Sea in 2018. The flux is positive for the transport from the sea to the atmosphere, while negative values refer to the transport from the atmosphere to the sea.

by a simultaneous local decrease in salinity and increase in pCO_2, was largest in August (Fig. 8c), when CO_2 concentrations locally exceeded saturation level, while in April and May–June, only a slight increase in pCO_2 relative to the surrounding waters was observed. In the GoR, river discharge is concentrated in the southern and eastern parts of the gulf (Yurkovskis et al., 1993). The influence of large rivers of the southern GoR was detected by a slight decrease in salinity in May–June and July, but a simultaneous increase in pCO_2 was observed only in May–June. The largest peaks, which could be linked to the river discharges, were associated with the Pärnu River, especially in April and May–June, when the background levels of pCO_2 in the adjacent regions were already low. Thus, the river waters influenced the observed pCO_2 patterns remarkably in the shallow and semi-enclosed Pärnu Bay and less in other areas.

Upwelling is the most prominent mesoscale process in the elongated GoF (Myrberg and Andrejev, 2003), where upwelling events along the southern coast are associated with north-easterly and easterly winds (Lips et al., 2009; Kikas and Lips, 2016). Winds supporting upwelling along the GoF southern coast dominated in October and also in July and late May, albeit with lower wind speed. In October, based on a comparison of salinity and temperature in the surface layer in the upwelling area and vertical profiles registered at the monitoring stations 2 d earlier, the upwelled waters mostly originated from the water layer of 65–75 m, i.e. the halocline. Most likely, the observed extreme pCO_2 values were caused by the relatively deep origin and the impact of the seabed when these waters were brought to the surface along the GoF slope.

In a case of upwelling in the Gotland Basin in July–August 2016, a very sharp increase in pCO_2 was measured, although the absolute values were lower than in our study (Jacobs et al., 2021). The authors evaluated the air–sea fluxes of CO_2 due to this upwelling event and showed that the CO_2 flux, expected to be directed from air into the sea in August, was reduced and even reversed due to upwelling. Kuss et al. (2006) have suggested that roughly 20 % of the annual CO_2 uptake in the central Arkona Sea could be balanced by CO_2 release during occasional upwelling events in the coastal areas, also considering seasonal differences in their impact. Similarly, Norman et al. (2013) estimated that upwelling events could possibly decrease the Baltic Sea's annual average CO_2 uptake by up to 25 %. In 2018, winds favouring upwelling along the northern coast of the GoF prevailed. However, we detected the upwelling events in the western GoF along the southern coast during cruises in late May and October. The highest pCO_2 values were recorded in upwelled waters in October when autumn mixing likely contributed to the vertical exchange, but it did not trigger production.

The seasonal course in pCO_2 in the surface layer is mainly controlled by the primary production in spring and summer and entrainment of waters with high pCO_2 due to remineralization processes during mixed-layer deepening in autumn (e.g. Schneider and Müller, 2018). The seasonal succession of phytoplankton, however, could be at different stages of development due to varying meteorological and hydrographic background along the 1500 km long measurement track (e.g. Seppälä and Balode, 1999; Lips et al., 2014). In April, the highest pCO_2 values, corresponding to the saturation level, observed in the parts of the GoR and GoF coincided with lower than the background Chl *a* and oxygen concentrations

(Fig. 5c and d). The lowest pCO_2 values were recorded in shallow areas with a warm surface layer with high Chl *a* concentrations. It is remarkable that in areas of high pCO_2, the sea surface temperature was 1–2 °C, meaning below the temperature of the maximum density of approximately 2.5 °C, and the water column was almost fully mixed, e.g. in the western and central GoR.

Like the stratification and bloom development in spring, the upper mixed layer deepening and stratification decay could shape the pCO_2 distribution patterns in the surface layer in late summer and autumn. By the August cruise, the upper mixed layer has been deepened to almost 30 m from the values of around 10 m in July. This resulted in high pCO_2 values in shallow areas (Fig. 8c), where the mixing has reached the bottom layer. However, the areas with higher pCO_2 values during summer cruises had CO_2 levels in October lower than in the deeper areas, where the mixing reached the near-bottom layer later, leaving less time for equilibration with the atmosphere in these deeper areas.

We suggest the following processes are responsible for the observed seasonal pattern in the Väinameri Sea (northern GoR) with an average depth of 5–10 m and relatively strong gradients of oceanographic variables (Suursaar et al., 2001). In April, pCO_2 levels were lower than in the adjacent deeper areas due to a warm surface layer and an earlier start of the spring bloom since the phytoplankton mixing depth in shallow areas is determined by the bottom depth and not vertical stratification (Townsend et al., 1994). In late May and July, the highest pCO_2 values were measured at the saltier side of the salinity front in the Väinameri Sea, likely favoured by weaker vertical stratification and, consequently, stronger vertical fluxes at the denser side of the fronts (e.g. Kahru et al., 1984). In August, the higher pCO_2 values in the shallow Väinameri Sea were likely related to the vertical mixing, and in October, when oversaturation was observed almost along the entire R/V track, pCO_2 was higher in other, deeper areas where the vertical flux (due to continuing upward mixing of deep, CO_2-rich waters) was still at a higher level, while a larger fraction of the CO_2 from the near-bottom layer had already been transported away from the Väinameri Sea.

Another area where saltier Baltic Proper and fresher GoR waters meet and the front develops is the Irbe Strait, conveying most of the GoR water exchange with the NBP (Lilover et al., 1998). Locally, the lowest pCO_2 was measured in connection to the Irbe front in April, probably due to the development of vertical stratification supporting the spring bloom, while in the GoR stratification was weak, and the bloom had not started yet. Contrarily, a slight local peak of pCO_2 in July could be caused by more intense vertical transport of sub-surface waters at the front.

5.1.2 cCH_4 distribution patterns

cCH_4 was oversaturated in the surface layer during the whole study period, which is typical for the Baltic Sea (Gülzow et al., 2013), with prominent local peaks in the GoF and GoR. These peaks can be related to the same physical processes as the local maxima in pCO_2 spatial distribution. However, two major peculiarities of cCH_4 distribution can be noticed – the local maximum values were more than an order of magnitude larger than the background cCH_4 level, and these prominent maxima were confined to the shallow areas. Although these peaks were not always observed in all shallow areas, this pattern agrees with the earlier results that methane concentrations and variability are high in shallow coastal areas (Roth et al., 2022; Borges et al., 2016).

Rivers have been identified as potentially strong sources of CH_4 in the Baltic Sea (Myllykangas et al., 2020), receiving CH_4 from soils, groundwater, wetlands, and floodplains in the watershed (De Angelis and Lilley, 1987; Richey et al., 1988). In April and May, elevated cCH_4 was measured near the Narva River mouth. However, the enhanced cCH_4 was also measured along the shallow coastal sea towards the west from the Narva River mouth. Similar distribution in August, with the maximum not at the mouth area but in the west, suggests that the river discharge was transported along the coast, as it could occur during summer months (Laanearu and Lips, 2003) or the shallowness and influence of sediments was the main factor creating this cCH_4 maximum. The latter suggestion or a combination of both would be the most likely explanation, since the water column was fully mixed along the ship track in this area.

Notable cCH_4 spatial variability emerged in the shallow Pärnu Bay, while cCH_4 values only slightly higher than the background were measured in the southern GoR. The research vessel track probably did not reach the river bulges properly in the southern GoR, or their influence was not seen offshore since the riverine waters were mostly transported along the coast (e.g. Lips et al., 2016b) and an anticyclonic river bulge was not formed as suggested by a modelling study (Soosaar et al., 2016). The highest cCH_4 peaks in the Pärnu Bay were observed in May and August (approximately 200 nmol L^{-1}), while in October, the peak was not so prominent, although the river discharge was larger than in summer months. In shallow coastal areas, high methane emissions have been linked to the amount of organic matter in the sediment and water temperature (e.g. Heyer and Berger, 2000). In addition, local maxima of cCH_4 were more pronounced in Pärnu Bay in comparison with the areas close to the Narva River mouth. We suggest that this pattern is related to the shallowness and semi-enclosed shape of Pärnu Bay and not directly to the changes in the river runoff.

The seafloor in most of the shallow bays is characterized by clay and mud or mixed sediments (mud and sand; EMODnet Geology, 2023), which are potential internal sources of methane (e.g. Humborg et al., 2019). This explains why cCH_4 peaks were recorded in these shallow areas where the water column was usually mixed down to the seabed. In October, when high cCH_4 values were also measured along the relatively deep south-western GoF (Fig. 9e), these findings

can be related to autumn vertical mixing and an intense upwelling event. A similar impact of upwelling has also been shown by earlier measurements in the Baltic Sea (Gülzow et al., 2013; Jacobs et al., 2021) and other coastal sea areas (e.g. Kock et al., 2008). It is noteworthy that our data show the impact of upwelling on surface CO_2 and CH_4 concentrations in fall, when upwelling was identified by salinity rather than temperature. Previous studies (Gülzow et al., 2013; Schneider et al., 2014; Jacobs et al., 2021) use the drop in sea surface temperature as an indicator for upwelling and upwelling-induced greenhouse gas fluxes, which bears the risk of underestimating the importance of upwelling for locally enhanced CO_2 and CH_4 fluxes in the Baltic in fall.

Elevated cCH_4 was almost always measured in the Väinameri Sea and can be explained by vertical mixing and resuspension of bottom sediments. Resuspension events occur due to wind mixing and waves but also due to frequently appearing strong currents in the straits (Suursaar et al., 2001; Otsmann et al., 2001). However, the detected cCH_4 peaks in the Väinameri Sea were not as strong as in Pärnu Bay, and in October a much higher cCH_4 peak was measured just outside of the Väinameri Sea in the upwelled waters in the south-western GoF (concentrations reached up to $70\,\mathrm{nmol\,L^{-1}}$; Fig. 9e). In the Irbe Strait, local cCH_4 maxima were also frequently observed. However, their locations were different from the observed pCO_2 extrema. We suggest that the cCH_4 maxima here were also related to the shallowest spots along the vessel track (either close to the Kolka or Sõrve peninsulas) and not to the Irbe front, as was observed for the observed pCO_2 peaks.

In summary, physically disturbed organic-rich sediments, river plumes, and upwelling were identified as processes causing hot spots of methane emission. While methane from undisturbed organic-rich sediments usually does not surpass effective anaerobic and aerobic methane oxidation in the upper sediment (e.g. Knittel and Boetius, 2009), physical shear stress can lead to the release of methane from the upper sediment layer. Borges et al. (2016) suggested water depth as a proxy for methane flux over organic-rich sediments in the North Sea. Similarly, our data support the importance of processes in shallow areas for assessing the CH_4 fluxes from the Baltic (and other marginal seas) to the atmosphere.

5.2 Comparison of seasonal variability between the basins

The temporal variations in pCO_2 in the surface layer of the NBP, GoF, and GoR in 2018 generally followed the known seasonal course (Thomas and Schneider, 1999; Schneider and Müller, 2018). In the Gotland Basin, the pCO_2 seasonal amplitude between 100 and 550 µatm has been registered (Schneider and Müller, 2018). In our study, the seasonal amplitude of pCO_2 was similar in all basins, with a slightly larger range in the GoF (50–1200 µatm). This higher amplitude is likely, at least in part, a result of the lower alkalinities in the GoF, which result in a higher pCO_2 change per amount of fixed carbon (e.g. Kuliński et al., 2017). The seasonal pCO_2 minimum in all basins appeared at the end of May when surface layer Chl *a* concentrations were already relatively low, as a result of the cumulative nature of the imprint of primary production on the inorganic carbon system. Our data did not reveal an increase in pCO_2 between the spring bloom and the cyanobacteria bloom in midsummer, which has been reported based on measurements with a higher temporal resolution (e.g. Schneider et al., 2014).

In the GoF and the GoR, Chl *a* concentrations in spring (Fig. 10e, Table 1) were higher than in the NBP, which is in accordance with the elevated nutrient concentrations in the GoF and GoR (HELCOM, 2018). However, a slightly higher average pCO_2 in the GoR during spring and summer could be related to the shallowness of this basin. Higher pCO_2 in the GoF in October and January can be explained by high biomass production in spring–summer and the specific hydrographic conditions supporting vertical transport and mixing of CO_2 from the deep layers in autumn–winter and during the upwelling events, in combination with the reduced buffering due to lower alkalinity in the GoF. High concentrations of inorganic carbon in the deep layers of the GoF result from the organic matter degradation in the presence of stratification in spring and summer and the advection of deep waters from the Baltic Proper (Lehtoranta et al., 2017). In late autumn and winter, collapses of vertical stratification could occur in the GoF (Liblik et al., 2013), resulting in the vertical transport of nutrients (and inorganic carbon) from the near-bottom layer to the surface layer (Lips et al., 2017). The high pCO_2 values attributed to upwelling in October in the GoF, also characterized by the lowest surface O_2 saturation of the entire survey, confirm active transport mechanisms of deep waters with strong biogeochemical indicators of mineralization of organic matter (Fig. 9c).

Since the GoR is shallower than the GoF and without a permanent halocline, CO_2 accumulation and subsequent CO_2 flux from the GoR deep layer do not have a similar high potential in autumn–winter to that in the GoF. However, the seasonal thermocline was stronger in spring–summer 2018 than on average due to high heat flux and calm wind conditions (Stoicescu et al., 2022). A near-bottom hypoxic layer developed, and the autumn–winter mixing had not reached the seabed in the deeper central GoR yet by the cruise in October (Stoicescu et al., 2022, also Fig. 9a). This could be a reason that relatively low pCO_2 was measured in the GoR while upwelling-related high values were recorded in the south-western GoF.

In our study, the second pCO_2 minimum in summer (or an increase between two minima) was not revealed, probably due to the long interval between cruises: 5 weeks between the cruises in late May–early June and mid-July and 5 weeks between the cruises in mid-July and the end of August. Summer cyanobacterial bloom in the GoF usually starts at the end of June or early July (Lips and Lips, 2008). Based on

our data from mid-July, calm wind conditions and high sea surface temperatures (median 17.7 °C, Table 1) favoured the bloom, which is also observable in an increase in Chl *a* concentration. Müller et al. (2021) showed that in 2018 in the eastern Gotland Basin, the production was intense from the beginning of their study period, 6 July (surface water pCO_2 was already as low as around 100 µatm), and *Nodularia* sp. peaked on 24 July, which is also the date of lowest pCO_2 values around 70 µatm. However, in the GoR, cyanobacteria biomass was 3 times lower in 2018 than in 2017 and a factor of 2 lower than the long-term mean (Kownacka et al., 2022).

cCH_4 dynamics in 2018 in the NBP, GoF and GoR followed the general seasonal cycle with the lowest methane concentrations in summer when thermal stratification hampers the methane transport from the deeper layers and the surface water gets depleted due to loss to the atmosphere by sea-air exchange, in part driven by the temperature-induced decreasing solubility. Gülzow et al. (2013) showed that the GoF surface water is characterized by elevated methane concentrations throughout the year (up to 22 nM in February) compared to offshore Baltic Sea regions. In our study, the NBP summer minimum remained within the comparable range with Gülzow et al. (2013), but the GoF summer minimum was twice as high. Note that we also covered the shallow southern coastal sea areas of the GoF with remarkable local peaks, while the GoF sub-transect by Gülzow et al. (2013) was almost fully located in the central Gulf of Finland.

Schmale et al. (2010) suggested that during summer elevated methane concentrations are observable in the GoF water column up to a depth of 20–30 m. Aerobic methane production has also been demonstrated to contribute to the slight oversaturation of surface waters in the central Baltic Sea (Schmale et al., 2018; Stawiarski et al., 2019), but the clear link between methane peaks in shallow areas and episodes of mixing reaching the seafloor suggests that these processes are of minor importance in our study area. Furthermore, the highest CH_4 concentrations observed in October 2018 in the south-western GoF could be a consequence of the specific hydrographic conditions – a combined effect of strong upwelling and autumn mixing.

In the GoR, sediments have a high organic matter content, and the area undergoes intermittent seasonal hypoxia (Stoicescu et al., 2022). In the shallow areas, likely wind-induced mixing remains relevant for the transport of methane from the sediment, including the potential for sediment resuspension and mobilization of methane-enriched pore waters. In April, the highest median cCH_4 was detected in the western and central parts of the GoR, where the water column was fully mixed down to the seabed. The seasonal stratification in the GoR during spring–summer 2018 was stronger than on average. It restricted vertical mixing and led to pronounced near-bottom oxygen depletion (Stoicescu et al., 2022) and probably to relatively low cCH_4 in the surface layer of the deeper GoR areas (where the seasonal thermocline existed).

5.3 Air–sea gas exchange

Several approaches have been used to assess whether the Baltic Sea is a sink or source of atmospheric CO_2, but no uniform consensus has been reached regarding the results (Dai et al., 2022). The estimation of fluxes on regional or global scales depends on the applied approaches, including whether pCO_2 data are calculated from other parameters (i.e. pH and total alkalinity) or direct pCO_2 measurements are conducted and whether model-based or remote sensing approaches are used (e.g. Wesslander et al., 2010; Schneider et al., 2014; Kuliński and Pempkowiak, 2011; Parard et al., 2017). In addition, most of the evaluations have been performed based on the data in the Baltic Proper (Gotland Basin; e.g. Thomas and Schneider, 1999; Schneider et al., 2014), and only a few studies have included data from the north-eastern sea areas (e.g. Honkanen et al., 2021). The results of our study generally show no major differences in the behaviour between the three analysed basins, except the high variability in the GoR and GoF that was likely observed since more shallow coastal areas were covered in these regions. It was also pointed out by Gutiérrez-Loza et al. (2021) that the fluxes in the Baltic Sea coastal regions were larger than in the offshore areas.

The CO_2 flux estimates (Table 2) show that the Estonian sea area was a source of atmospheric CO_2 during the winter and autumn and a sink during the spring and summer of 2018. In addition, the estimates suggest that all studied subbasins were CO_2 sinks on an annual basis. However, due to the high temporal and spatial variability and the fact that the six cruises were distributed unevenly across the year, with bi-monthly gaps between the measurements in autumn and winter, it cannot be conclusively defined whether the area is a source or a sink over the course of the year.

In our study, the estimated annual mean flux in the NBP was $-0.06\,\mathrm{g\,C\,m^{-2}\,d^{-1}}$ ($-1.8\,\mathrm{mol\,m^{-2}\,yr^{-1}}$). Flux estimates for 2005, 2008, and 2009 by Schneider et al. (2014) showed that the central and northern Gotland Basin areas act as a net sink for atmospheric CO_2, with uptake rates ranging between -0.60 and $-0.89\,\mathrm{mol\,m^{-2}\,yr^{-1}}$. Several factors may account for these differences in flux estimates. The summer of 2018 could have been more productive due to warm weather conditions. On the other hand, our measurements covered the transition areas NBP–GoF and NBP–GoR, where the fluctuations in fluxes are greater than in offshore areas analysed in the study by Schneider et al. (2014). Müller et al. (2021) concluded that their observations in the eastern Gotland Basin in July–August 2018 were representative of Baltic Sea cyanobacteria blooms in general, although the pCO_2 levels in 2018 varied between the upper and lower ends of the conditions observed in previous years (Schneider and Müller, 2018). Additionally, the difference in flux estimates might be caused by different parameterizations used (Wesslander et al., 2011).

The calculated annual mean fluxes in the GoF and GoR were smaller than in the NBP. An analysis of these values in

more detail (Table 2) reveals that CO_2 uptake during spring–summer was the greatest in the GoF (Fig. 11a). As a counterbalance to summer absorption, the CO_2 release in October had a large impact on the estimates of the annual mean fluxes. In the NBP, the impact of the autumn release was smaller (Table 2), but it was significant for the GoF and GoR annual mean flux estimates due to the upwelling event along the southern coast of the GoF and the shallower basin with mixing reaching the seabed in most of the GoR.

The Baltic Sea is a source of atmospheric CH_4 and shows strong spatial and seasonal variations (Bange et al., 1994; Gülzow et al., 2013). In addition, the present dataset shows that the Estonian sea area is a source of atmospheric CH_4 during spring, summer, and autumn (Table 3; Fig. 11b). A considerable increase in the calculated methane flux was observed in August, as detected by Gülzow et al. (2013), who explained such an increase as a consequence of the transition to the regime of high wind velocities. Due to the upwelling event in October, methane outgassing in our study was probably intensified in autumn (Jacobs et al., 2021). The calculated CH_4 fluxes in the NBP (Table 3; Fig. 11b) were much lower and much less variable than in the GoF and GoR. The reason is similar to that discussed regarding the CO_2 fluxes: more shallow coastal areas were covered in the GoF and GoR than in the NBP.

For a robust flux estimate in the entire (north-eastern) Baltic Sea, understanding and monitoring of coastal processes seem to be mandatory in addition to measurements in the central Baltic – even when integrating over the surface area. On the other hand, even a few data from the NBP would likely be representative of a very large area, given the error ranges.

6 Conclusions

Spatial patterns and seasonal dynamics of CO_2 and CH_4 were studied in the north-eastern Baltic Sea area. We observed that the southern GoF and GoR have considerably higher spatial variability and seasonal amplitude of surface layer pCO_2 and cCH_4 than what has been measured in the offshore areas of the Baltic Sea (pCO_2 50–1200 µatm vs. 100–550 µatm, respectively; cCH_4 80 vs. 22 nmol L^{-1}, respectively). The main processes behind this high variability are coastal upwelling events, hydrographic fronts (e.g. Irbe front), mixing reaching the seabed, and possible shifts in the timing of bloom events influenced by hydrography. On average, the CO_2 air–sea fluxes in the north-eastern Baltic Sea are similar between the sub-basins but with larger amplitudes in the coastal areas. However, regional variations in CO_2 dynamics also result in differences in annual flux estimates between the sub-basins.

Due to the observed high variability, it is recommended to continue similar high-resolution measurements in the coastal and offshore areas at least every season during the regular environmental monitoring cruises. It is essential for accurately evaluating the role of this region in the Baltic Sea carbon budget and to predict potential future changes due to anthropogenic or climatic pressures. Additionally, high-resolution pCO_2 measurements have a strong potential to contribute to eutrophication monitoring, enabling quantitative assessment of organic matter production and mineralization (Schneider and Müller, 2018), and they can be used as a pivotal parameter to trace acidification (Gustafsson et al., 2023).

Data availability. The dataset is available at https://doi.org/10.48726/t22h5-jkx78 (Lainela et al., 2024).

Author contributions. SL, EJ, GR, and UL conceived the study. UL contributed to developing methods and writing the manuscript. GR contributed to developing methods and reviewing the manuscript. EJ contributed by analysing the data and writing and reviewing the manuscript. STL contributed by analysing and visualizing the data and reviewing the manuscript. SL carried out analyses, prepared the figures, and wrote the manuscript with editorial and scientific contributions from all co-authors.

Competing interests. The contact author has declared that none of the authors has any competing interests.

Disclaimer. Publisher's note: Copernicus Publications remains neutral with regard to jurisdictional claims made in the text, published maps, institutional affiliations, or any other geographical representation in this paper. While Copernicus Publications makes every effort to include appropriate place names, the final responsibility lies with the authors.

Acknowledgements. The authors would like to thank Michael Glockzin for his contribution and support with the trace gas measurements, Villu Kikas for his technical assistance, and the crew of the R/V *Salme* for their help and cooperation. Silvie Lainela's sincere words of thanks also go to our TalTech colleagues Sander Rikka and Ilja Maljutenko for the fruitful discussions in developing and optimizing Python and MATLAB scripts and Germo Väli for his help and advice regarding meteorological data.

Financial support. The study was done within the framework of the BONUS INTEGRAL project (grant no. 03F0773A), which received funding from BONUS (Art 185), funded jointly by the EU, the German Federal Ministry of Education and Research, the Swedish Research Council Formas, the Academy of Finland, the Polish National Centre for Research and Development, and the Estonian Research Council. The work of Silvie Lainela, Stella-Theresa Luik, and Urmas Lips was supported by the Estonian Research Council (grant no. PRG602). The analysis was also partly supported by the JERICO-S3 project (funded by the European Commission's Hori-

zon 2020 Research and Innovation programme under grant agreement nos. 871153 and 951799).

Review statement. This paper was edited by Hermann Bange and reviewed by two anonymous referees.

References

Alenius, P., Myrberg, K., and Nekrasov, A.: The physical oceanography of the Gulf of Finland: a review, Boreal Environ. Res., 3, 97–125, 1998.

Alenius, P., Nekrasov, A., and Myrberg, K.: Variability of the baroclinic Rossby radius in the Gulf of Finland, Cont. Shelf Res., 23, 563–573, https://doi.org/10.1016/S0278-4343(03)00004-9, 2003.

Andrejev, O., Myrberg, K., Alenius, P., and Lundberg, P.A.: Mean circulation and water exchange in the Gulf of Finland e a study based on three-dimensional modelling, Boreal. Environ. Res., 9, 1–16, 2004.

Astok, V., Otsmann, M., and Suursaar, Ü.: Water exchange as the main physical process in semi-enclosed marine systems: the Gulf of Riga case, Hydrobiologia, 393, 11–18, https://doi.org/10.1023/A:1003517110726, 1999.

Bange, H. W., Bartell, U. H., Rapsomanikis, S., and Andreae, M. O.: Methane in the Baltic and North Seas and a reassessment of the marine emissions of methane, Global Biogeochem. Cy., 8, 465–480, https://doi.org/10.1029/94GB02181, 1994.

Borges, A. V., Champenois, W., Gypens, N., Delille, B., and Harlay, J.: Massive marine methane emissions from near-shore shallow coastal areas, Sci. Rep.-UK, 6, 27908, https://doi.org/10.1038/srep27908, 2016.

Borges, A. V., Speeckaert, G., Champenois, W., Scranton, M. I., and Gypens, N.: Productivity and Temperature as Drivers of Seasonal and Spatial Variations of Dissolved Methane in the Southern Bight of the North Sea, Ecosystems, 21, 583–599, https://doi.org/10.1007/s10021-017-0171-7, 2018.

Canadell, J. G., Monteiro, P. M. S., Costa, M. H., Cotrim da Cunha, L., Cox, P. M., Eliseev, A. V., Henson, S., Ishii, M., Jaccard, S., Koven, C., Lohila, A., Patra, P. K., Piao, S., Rogelj, J., Syampungani, S., Zaehle, S., and Zickfeld, K.: Global Carbon and other Biogeochemical Cycles and Feedbacks, in: Climate Change 2021 – The Physical Science Basis, Contribution of Working Group I to the Sixth Assessment Report of the Intergovernmental Panel on Climate Change, edited by: Masson-Delmotte, V., Zhai, P., Pirani, A., Connors, S. L., Péan, C., Berger, S., Caud, N., Chen, Y., Goldfarb, L., Gomis, M. I., Huang, M., Leitzell, K., Lonnoy, E., Matthews, J. B. R., Maycock, T. K., Waterfield, T., Yelekçi, O., Yu, R., and Zhou, B., Cambridge University Press, 673–816, https://doi.org/10.1017/9781009157896.007, 2023.

Dai, M., Su, J., Zhao, Y., Hofmann, E.E., Cao, Z., Cai, W.-J., Gan, J., Lacroix, F., Laruelle, G. G., Meng, F., Müller, J. D., Regnier, P. A. G., Wang, G., and Wang, Z.: Carbon Fluxes in the Coastal Ocean: Synthesis, Boundary Processes, and Future Trends, Annu. Rev. Earth Pl. Sc., 50, 593–626, https://doi.org/10.1146/annurev-earth-032320-090746, 2022.

De Angelis, M. A. and Lilley, M. D.: Methane in surface waters of Oregon estuaries and rivers, Limnol. Oceanogr., 32, 716–722, https://doi.org/10.4319/lo.1987.32.3.0716, 1987.

Dlugokencky, E. J., Steele, L. P., Lang, P. M., and Masarie, K. A.: The growth rate and distribution of atmospheric methane, J. Geophys. Res., 99, 17021–17043, https://doi.org/10.1029/94JD01245, 1994.

EMODnet Geology: https://emodnet.ec.europa.eu/geoviewer/?layers=12494:1:1&basemap=ebwbl&active=12494&bounds=1889347.1962289177,7790646.9624039605,3305342.315828531,8401847.980824888&filters=&projection=EPSG:3857, last access: 25 August 2023.

Friedlingstein, P., O'Sullivan, M., Jones, M. W., Andrew, R. M., Gregor, L., Hauck, J., Le Quéré, C., Luijkx, I. T., Olsen, A., Peters, G. P., Peters, W., Pongratz, J., Schwingshackl, C., Sitch, S., Canadell, J. G., Ciais, P., Jackson, R. B., Alin, S. R., Alkama, R., Arneth, A., Arora, V. K., Bates, N. R., Becker, M., Bellouin, N., Bittig, H. C., Bopp, L., Chevallier, F., Chini, L. P., Cronin, M., Evans, W., Falk, S., Feely, R. A., Gasser, T., Gehlen, M., Gkritzalis, T., Gloege, L., Grassi, G., Gruber, N., Gürses, Ö., Harris, I., Hefner, M., Houghton, R. A., Hurtt, G. C., Iida, Y., Ilyina, T., Jain, A. K., Jersild, A., Kadono, K., Kato, E., Kennedy, D., Klein Goldewijk, K., Knauer, J., Korsbakken, J. I., Landschützer, P., Lefèvre, N., Lindsay, K., Liu, J., Liu, Z., Marland, G., Mayot, N., McGrath, M. J., Metzl, N., Monacci, N. M., Munro, D. R., Nakaoka, S.-I., Niwa, Y., O'Brien, K., Ono, T., Palmer, P. I., Pan, N., Pierrot, D., Pocock, K., Poulter, B., Resplandy, L., Robertson, E., Rödenbeck, C., Rodriguez, C., Rosan, T. M., Schwinger, J., Séférian, R., Shutler, J. D., Skjelvan, I., Steinhoff, T., Sun, Q., Sutton, A. J., Sweeney, C., Takao, S., Tanhua, T., Tans, P. P., Tian, X., Tian, H., Tilbrook, B., Tsujino, H., Tubiello, F., van der Werf, G. R., Walker, A. P., Wanninkhof, R., Whitehead, C., Willstrand Wranne, A., Wright, R., Yuan, W., Yue, C., Yue, X., Zaehle, S., Zeng, J., and Zheng, B.: Global Carbon Budget 2022, Earth Syst. Sci. Data, 14, 4811–4900, https://doi.org/10.5194/essd-14-4811-2022, 2022.

Gustafsson, E., Carstensen, J., Fleming, V., Gustafsson, B. G., Hoikkala, L., and Rehder, G.: Causes and consequences of acidification in the Baltic Sea: implications for monitoring and management, Sci. Rep.-UK, 13, 16322, https://doi.org/10.1038/s41598-023-43596-8, 2023.

Gutiérrez-Loza, L., Wallin, M. B., Sahlée, E., Holding, T., Shutler, J. D., Rehder, G., and Rutgersson, A.: Air–sea CO_2 exchange in the Baltic Sea–A sensitivity analysis of the gas transfer velocity, J. Marine Syst., 222, 103603, https://doi.org/10.1016/j.jmarsys.2021.103603, 2021.

Gülzow, W., Rehder, G., Schneider, B., Schneider von Deimling, J., and Sadkowiak, B.: A new method for continuous measurement of methane and carbon dioxide in surface waters using off-axis integrated cavity output spectroscopy (ICOS): An example from the Baltic Sea, Limnol. Oceanogr.-Meth., 9, 176–184, https://doi.org/10.4319/lom.2011.9.176, 2011.

Gülzow, W., Rehder, G., Schneider v. Deimling, J., Seifert, T., and Tóth, Z.: One year of continuous measurements constraining methane emissions from the Baltic Sea to the atmosphere using a ship of opportunity, Biogeosciences, 10, 81–99, https://doi.org/10.5194/bg-10-81-2013, 2013.

Gülzow, W., Gräwe, U., Kedzior, S., Schmale, O., and Rehder, G.: Seasonal variation of methane in the water column of Arkona

and Bornholm Basin, western Baltic Sea, J. Marine Syst., 139, 332–347, https://doi.org/10.1016/j.jmarsys.2014.07.013, 2014.

HELCOM: Manual for the Marine Monitoring in the COMBINE Programme of HELCOM, https://helcom.fi/action-areas/monitoring-and-assessment/monitoring-guidelines/combine-manual/ (last access: 16 June 2023), 2017.

HELCOM: HELCOM Thematic assessment of eutrophication 2011–2016. Baltic Sea Environment Proceedings No. 156, Baltic Marine Environment Protection Commission, ISSN 0357-2994, 2018.

Hersbach, H., Bell, B., Berrisford, P., Biavati, G., Horányi, A., Muñoz Sabater, J., Nicolas, J., Peubey, C., Radu, R., Rozum, I., Schepers, D., Simmons, A., Soci, C., Dee, D., and Thépaut, J.-N.: ERA5 monthly averaged data on single levels from 1979 to present, Copernicus Climate Change Service (C3S) Climate Data Store (CDS) [data set], https://doi.org/10.24381/cds.f17050d7, 2019.

Heyer, J. and Berger, U.: Methane emission from the coastal area in the southern Baltic Sea, Estuar. Coast. Shelf S., 51, 13–30, https://doi.org/10.1006/ecss.2000.0616, 2000.

Holding, T., Ashton, I. G., Shutler, J. D., Land, P. E., Nightingale, P. D., Rees, A. P., Brown, I., Piolle, J.-F., Kock, A., Bange, H. W., Woolf, D. K., Goddijn-Murphy, L., Pereira, R., Paul, F., Girard-Ardhuin, F., Chapron, B., Rehder, G., Ardhuin, F., and Donlon, C. J.: The FluxEngine air–sea gas flux toolbox: simplified interface and extensions for in situ analyses and multiple sparingly soluble gases, Ocean Sci., 15, 1707–1728, https://doi.org/10.5194/os-15-1707-2019, 2019.

Honkanen, M., Müller, J. D., Seppälä, J., Rehder, G., Kielosto, S., Ylöstalo, P., Mäkelä, T., Hatakka, J., and Laakso, L.: The diurnal cycle of pCO_2 in the coastal region of the Baltic Sea, Ocean Sci., 17, 1657–1675, https://doi.org/10.5194/os-17-1657-2021, 2021.

Hoy, A., Hänsel, S., and Maugeri, M.: An endless summer: 2018 heat episodes in Europe in the context of secular temperature variability and change, Int. J. Climatol., 40, 6315–6336, https://doi.org/10.1002/joc.6582, 2020.

Humborg, C., Geibel, M. C., Sun, X., McCrackin, M., Mörth, C.-M., Stranne, C., Jakobsson, M., Gustafsson, B., Sokolov, A., Norkko, A., and Norkko, J.: High Emissions of Carbon Dioxide and Methane From the Coastal Baltic Sea at the End of a Summer Heat Wave, Front. Mar. Sci., 6, 493, https://doi.org/10.3389/fmars.2019.00493, 2019.

IOC, SCOR and IAPSO: The International Thermodynamic Equation of Seawater – 2010: Calculation and Use of Thermodynamic Properties, Intergovernmental Oceanographic Commission, Manuals and Guides No. 56, UNESCO, 196 pp., 2010.

Jacobs, E., Bittig, H. C., Gräwe, U., Graves, C. A., Glockzin, M., Müller, J. D., Schneider, B., and Rehder, G.: Upwelling-induced trace gas dynamics in the Baltic Sea inferred from 8 years of autonomous measurements on a ship of opportunity, Biogeosciences, 18, 2679–2709, https://doi.org/10.5194/bg-18-2679-2021, 2021.

Jakobs, G., Rehder, G., Jost, G., Kießlich, K., Labrenz, M., and Schmale, O.: Comparative studies of pelagic microbial methane oxidation within the redox zones of the Gotland Deep and Landsort Deep (central Baltic Sea), Biogeosciences, 10, 7863–7875, https://doi.org/10.5194/bg-10-7863-2013, 2013.

Jakobs, G., Holtermann, P., Berndmeyer, C., Rehder, G., Blumenberg, M., Jost, G., Nausch, G., and Schmale, O.: Seasonal and spatial methane dynamics in the water column of the central Baltic Sea (Gotland Sea), Cont. Shelf Res., 91, 12–25, https://doi.org/10.1016/j.csr.2014.07.005, 2014.

Kahru, M., Elken, J., Kotta, I., Simm, M., and Vilbaste, K.: Plankton distributions and processes across a front in the open Baltic sea, Mar. Ecol. Prog. Ser., 20, 101–111, 1984.

Keeling, R. F., Piper, S. C., Bollenbacher, A. F., and Walker, J. S.: Atmospheric Carbon Dioxide Record from Mauna Loa, CDIAC, ESS-DIVE repository [data set], https://doi.org/10.3334/CDIAC/ATG.035, 2009.

Kikas, V. and Lips, U.: Upwelling characteristics in the Gulf of Finland (Baltic Sea) as revealed by Ferrybox measurements in 2007–2013, Ocean Sci., 12, 843–859, https://doi.org/10.5194/os-12-843-2016, 2016.

Knittel, K. and Boetius, A.: Anaerobic oxidation of methane: progress with an unknown process, Annu. Rev. Microbiol., 63, 311–334, https://doi.org/10.1146/annurev.micro.61.080706.093130, 2009.

Kock, A., Gebhardt, S., and Bange, H. W.: Methane emissions from the upwelling area off Mauritania (NW Africa), Biogeosciences, 5, 1119–1125, https://doi.org/10.5194/bg-5-1119-2008, 2008.

Kownacka, J., Busch, S., Göbel, J., Gromisz, S., Hällfors, H., Höglander, H., Huseby, S., Jaanus, A., Jakobsen, H. H., Johansen, M., Johansson, M., Jurgensone, I., Liebeke, N., Kobos, J., Kraśniewski, W., Kremp, A., Lehtinen, S., Olenina, I., v. Weber, M., and Wasmund, N.: Cyanobacteria biomass, 1990–2019, HELCOM Balt, Sea Environ. Fact Sheets, Online, Helsinki Commission, https://helcom.fi/wp-content/uploads/2022/04/BSEFS-Cyanobacteria-biomass-1990-2020.pdf (last access: 16 June 2023), 2022.

Kuliński, K. and Pempkowiak, J.: The carbon budget of the Baltic Sea, Biogeosciences, 8, 3219–3230, https://doi.org/10.5194/bg-8-3219-2011, 2011.

Kuliński, K., Schneider, B., Szymczycha, B., and Stokowski, M.: Structure and functioning of the acid–base system in the Baltic Sea, Earth Syst. Dynam., 8, 1107–1120, https://doi.org/10.5194/esd-8-1107-2017, 2017.

Kuss, J., Roeder, W., Wlost, K.-P., and DeGrandpre, M.D.: Time-series of surface water CO_2 and oxygen measurements on a platform in the central Arkona Sea (Baltic Sea): Seasonality of uptake and release, Mar. Chem., 101, 220–232, https://doi.org/10.1016/j.marchem.2006.03.004, 2006.

Laanearu, J. and Lips, U.: Observed thermohaline fields and low-frequency currents in the Narva Bay, Proceedings of the Estonian Academy of Sciences Engineering, 9, 91–106, 2003.

Lainela, S., Jacobs, E., Luik, S.-T., Rehder, G., and Lips, U.: Seasonal dynamics and regional distribution patterns of CO2 and CH4 in the north-eastern Baltic Sea, TalTech Data Repository [data set], https://doi.org/10.48726/t22h5-jkx78, 2024.

Lehtoranta, J., Savchuk, O. P., Elken, J., Kim, D., Kuosa, H., Raateoja, M., Kauppila, P., Räike, A., and Pitkänen, H.: Atmospheric forcing controlling inter-annual nutrient dynamics in the open Gulf of Finland, J. Marine Syst., 171, 4–20, 2017.

Leppäranta, M. and Myrberg, K.: Physical Oceanography of the Baltic Sea, Springer Science & Business Media, 378 pp., ISBN 3540797033, 2009.

Liblik, T. and Lips, U.: Variability of synoptic-scale quasi-stationary thermohaline stratification patterns in the Gulf

of Finland in summer 2009, Ocean Sci., 8, 603–614, https://doi.org/10.5194/os-8-603-2012, 2012.

Liblik, T., Laanemets, J., Raudsepp, U., Elken, J., and Suhhova, I.: Estuarine circulation reversals and related rapid changes in winter near-bottom oxygen conditions in the Gulf of Finland, Baltic Sea, Ocean Sci., 9, 917–930, https://doi.org/10.5194/os-9-917-2013, 2013.

Liblik, T., Väli, G., Salm, K., Laanemets, J., Lilover, M.-J., and Lips, U.: Quasi-steady circulation regimes in the Baltic Sea, Ocean Sci., 18, 857–879, https://doi.org/10.5194/os-18-857-2022, 2022.

Lilover, M. J., Lips, U., Laanearu, J., and Liljebladh, B.: Flow regime in the Irbe Strait, Aquat. Sci., 60, 253–265, 1998.

Lips, I. and Lips, U.: Abiotic factors influencing cyanobacterial bloom development in the Gulf of Finland (Baltic Sea), Hydrobiologia, 614, 133–140, https://doi.org/10.1007/s10750-008-9449-2, 2008.

Lips, I., Lips, U., and Liblik, T.: Consequences of coastal upwelling events on physical and chemical patterns in the central Gulf of Finland (Baltic Sea), Cont. Shelf Res., 29, 1836–1847, https://doi.org/10.1016/j.csr.2009.06.010, 2009.

Lips, I., Rünk, N., Kikas, V., Meerits, A., and Lips, U.: High-resolution dynamics of the spring bloom in the Gulf of Finland of the Baltic Sea, J. Marine Syst., 129, 135–149, https://doi.org/10.1016/j.jmarsys.2013.06.002, 2014.

Lips, U., Kikas, V., Liblik, T., and Lips, I.: Multi-sensor in situ observations to resolve the sub-mesoscale features in the stratified Gulf of Finland, Baltic Sea, Ocean Sci., 12, 715–732, https://doi.org/10.5194/os-12-715-2016, 2016a.

Lips, U., Zhurbas, V., Skudra, M., and Väli, G.: A numerical study of circulation in the Gulf of Riga, Baltic Sea. Part I: Whole-basin gyres and mean currents, Cont. Shelf Res., 112, 1–13, https://doi.org/10.1016/j.csr.2015.11.008, 2016b.

Lips, U., Laanemets, J., Lips, I., Liblik, T., Suhhova, I., and Suursaar, Ü.: Wind-driven residual circulation and related oxygen and nutrient dynamics in the Gulf of Finland (Baltic Sea) in winter, Estuar. Coast. Shelf S., 195, 4–15, https://doi.org/10.1016/j.ecss.2016.10.006, 2017.

Maljutenko, I. and Raudsepp, U.: Long-term mean, interannual and seasonal circulation in the Gulf of Finland – The wide salt wedge estuary or gulf type ROFI, J. Marine Syst., 195, 1–19, https://doi.org/10.1016/j.jmarsys.2019.03.004, 2019.

Müller, J. D., Schneider, B., and Rehder, G.: Long-term alkalinity trends in the Baltic Sea and their implications for CO_2-induced acidification, Limnol. Oceanogr., 61, 1984–2002, https://doi.org/10.1002/lno.10349, 2016.

Müller, J. D., Schneider, B., Gräwe, U., Fietzek, P., Wallin, M. B., Rutgersson, A., Wasmund, N., Krüger, S., and Rehder, G.: Cyanobacteria net community production in the Baltic Sea as inferred from profiling pCO_2 measurements, Biogeosciences, 18, 4889–4917, https://doi.org/10.5194/bg-18-4889-2021, 2021.

Myllykangas, J. P., Hietanen, S., and Jilbert, T.: Legacy effects of eutrophication on modern methane dynamics in a boreal estuary, Estuar. Coasts, 43, 189–206, https://doi.org/10.1007/s12237-019-00677-0, 2020.

Myrberg, K. and Andrejev, O.: Main upwelling regions in the Baltic Sea – a statistical analysis based on three-dimensional modelling, Boreal Environ. Res., 8, 97–112, 2003.

Nightingale, P. D., Malin, G., Law, C. S., Watson, A. J., Liss, P. S., Liddicoat, M. I., Boutin, J., and Upstill-Goddard, R. C.: In situ evaluation of air-sea gas exchange parameterizations using novel conservative and volatile tracers, Global Biogeochem. Cy., 14, 373–387, https://doi.org/10.1029/1999GB900091, 2000.

Norman, M., Parampil, S. R., Rutgersson, A., and Sahlée, E.: Influence of coastal upwelling on the air–sea gas exchange of CO_2 in a Baltic Sea Basin, Tellus B, 65, 21831, https://doi.org/10.3402/tellusb.v65i0.21831, 2013.

Ojaveer, E. (Ed.): Ecosystem of the Gulf of Riga between 1920 and 1990, Estonian Academy Publishers, Tallinn, 277 pp., ISBN 9985500652, 1995.

Otsmann, M., Suursaar, Ü., and Kullas, T.: The oscillatory nature of the flows in the system of straits and small semienclosed basins of the Baltic Sea, Cont. Shelf Res., 21, 1577–1603, https://doi.org/10.1016/S0278-4343(01)00002-4, 2001.

Parard, G., Rutgersson, A., Raj Parampil, S., and Charantonis, A. A.: The potential of using remote sensing data to estimate air–sea CO_2 exchange in the Baltic Sea, Earth Syst. Dynam., 8, 1093–1106, https://doi.org/10.5194/esd-8-1093-2017, 2017.

Pavelson, J.: Mesoscale physical processes and the related impact on the summer nutrient fields and phytoplankton blooms in the western Gulf of Finland, PhD thesis, Department of Marine Systems, Tallinn University of Technology, Estonia, 38 pp., ISBN 9985595564, 2005.

Placke, M., Meier, H. E. M., Gräwe, U., Neumann, T., Frauen, C., and Liu, Y.: Long-Term Mean Circulation of the Baltic Sea as Represented by Various Ocean Circulation Models, Front. Mar. Sci., 5, 287, https://doi.org/10.3389/fmars.2018.00287, 2018.

Reeburgh, W. S.: Oceanic methane biogeochemistry, Chem. Rev., 107, 486–513, https://doi.org/10.1021/cr050362v, 2007.

Richey, J. E., Devol, A. H., Wofsy, S. C., Victoria, R., and Riberio, M. N.: Biogenic gases and the oxidation and reduction of carbon in Amazon River and floodplain waters, Limnol. Oceanogr., 33, 551–561, https://doi.org/10.4319/lo.1988.33.4.0551, 1988.

Roth, F., Sun, X., Geibel, M. C., Prytherch, J., Brüchert, V., Bonaglia, S., Broman, E., Nascimento, F., Norkko, A., and Humborg, C.: High spatiotemporal variability of methane concentrations challenges estimates of emissions across vegetated coastal ecosystems, Glob. Change Biol., 28, 4308–4322, https://doi.org/10.1111/gcb.16177, 2022.

Sabbaghzadeh, B., Arévalo-Martínez, D. L., Glockzin, M., Otto, S., and Rehder, G.: Meridional and Cross-Shelf Variability of N_2O and CH_4 in the Eastern-South Atlantic, J. Geophys. Res.-Oceans, 126, e2020JC016878, https://doi.org/10.1029/2020JC016878, 2021.

Schmale, O., Schneider v. Deimling, J., Gülzow, W., Nausch, G., Waniek, J. J., and Rehder, G.: Distribution of methane in the water column of the Baltic Sea, Geophys. Res. Lett., 37, L12604, https://doi.org/10.1029/2010GL043115, 2010.

Schmale, O., Wäge, J., Mohrholz, V., Wasmund, N., Gräwe, U., Rehder, G., Labrenz, M., and Loick-Wilde, N.: The contribution of zooplankton to methane supersaturation in the oxygenated upper waters of the central Baltic Sea, Limnol. Oceanogr., 63, 412–430, https://doi.org/10.1002/lno.10640, 2018.

Schneider, B. and Müller, J. D.: Biogeochemical Transformations in the Baltic Sea, Springer Oceanography, Springer International Publishing, Cham, Switzerland, https://doi.org/10.1007/978-3-319-61699-5, 2018.

Schneider, B., Gülzow, W., Sadkowiak, B., and Rehder, G.: Detecting sinks and sources of CO2 and CH4 by ferrybox-based measurements in the Baltic Sea: Three case studies, J. Marine Syst., 140, 13–25, https://doi.org/10.1016/j.jmarsys.2014.03.014, 2014.

Seppälä, J. and Balode, M.: Spatial distribution of phytoplankton in the Gulf of Riga during spring and summer stages, J. Marine Syst., 23, 51–67, https://doi.org/10.1016/S0924-7963(99)00050-0, 1999.

Shutler, J. D., Land, P. E., Piolle, J. F., Woolf, D. K., Goddijn-Murphy, L., Paul, F., Girard-Ardhuin, F., Chapron, B., and Donlon, C. J.: FluxEngine: a flexible processing system for calculating atmosphere-ocean carbon dioxide gas fluxes and climatologies, J. Atmos. Ocean. Tech., 33, 741–756, https://doi.org/10.1175/JTECH-D-14-00204.1, 2016.

Skudra, M. and Lips, U.: Characteristics and inter-annual changes in temperature, salinity and density distribution in the Gulf of Riga, Oceanologia, 59, 37–48, https://doi.org/10.1016/j.oceano.2016.07.001, 2017.

Soosaar, E., Maljutenko, I., Uiboupin, R., Skudra, M., and Raudsepp, U.: River bulge evolution and dynamics in a non-tidal sea – Daugava River plume in the Gulf of Riga, Baltic Sea, Ocean Sci., 12, 417–432, https://doi.org/10.5194/os-12-417-2016, 2016.

Stawiarski, B., Otto, S., Thiel, V., Gräwe, U., Loick-Wilde, N., Wittenborn, A. K., Schloemer, S., Wäge, J., Rehder, G., Labrenz, M., Wasmund, N., and Schmale, O.: Controls on zooplankton methane production in the central Baltic Sea, Biogeosciences, 16, 1–16, https://doi.org/10.5194/bg-16-1-2019, 2019.

Stålnacke, P., Grimvall, A., Sundblad, K., and Tonderski, A.: Estimation of riverine loads of nitrogen and phosphorus to the Baltic Sea, 1970–1993, Environ. Monit. Assess., 58, 173–200, https://doi.org/10.1023/A:1006073015871, 1999.

Stiebrins, O. and Väling, P.: Bottom sediments of the Gulf of Riga, Geol. Surv. Latv. Riga, 4 pp., ISBN 9984-9130-0-7, 1996.

Stoicescu, S.-T., Lips, U., and Liblik, T.: Assessment of Eutrophication Status Based on Sub-Surface Oxygen Conditions in the Gulf of Finland (Baltic Sea), Front. Mar. Sci., 6, 54, https://doi.org/10.3389/fmars.2019.00054, 2019.

Stoicescu, S.-T., Laanemets, J., Liblik, T., Skudra, M., Samlas, O., Lips, I., and Lips, U.: Causes of the extensive hypoxia in the Gulf of Riga in 2018, Biogeosciences, 19, 2903–2920, https://doi.org/10.5194/bg-19-2903-2022, 2022.

Suursaar, Ü., Kullas, T., and Otsmann, M.: The influence of currents and waves on ecological conditions of the Väinameri, Proceedings of the Estonian Academy of Sciences Biology Ecology, 50, 231–247, 2001.

Takahashi, T., Olafsson, J., Goddard, J. G., Chipman, D. W., and Sutherland, S. C.: Seasonal variation of CO_2 and nutrients in the high-latitude surface oceans: A comparative study, Global Biogeochem. Cy., 7, 843–878, https://doi.org/10.1029/93GB02263, 1993.

Thomas, H. and Schneider, B.: The seasonal cycle of carbon dioxide in Baltic Sea surface waters, J. Marine Syst., 22, 53–67, https://doi.org/10.1016/S0924-7963(99)00030-5, 1999.

Townsend, D. W., Cammen, L. M., Holligan, P. M., Campbell, D., and Pettigrew, N. R.: Causes and consequences of variability in the timing of spring phytoplankton blooms, Deep-Sea Res. Pt. I, 41, 747–765, https://doi.org/10.1016/0967-0637(94)90075-2, 1994.

Valentine, D. L.: Biogeochemistry and microbial ecology of methane oxidation in anoxic environments: a review, A. Van Leeuw. J. Mocrob., 81, 271–282, https://doi.org/10.1023/A:1020587206351, 2002.

Wanninkhof, R.: Relationship between wind speed and gas exchange over the ocean revisited, Limnol. Oceanogr.-Meth., 12, 351–362, https://doi.org/10.4319/lom.2014.12.351, 2014.

Weber, T., Wiseman, N. A., and Kock, A.: Global ocean methane emissions dominated by shallow coastal waters, Nat. Commun., 10, 4584, https://doi.org/10.1038/s41467-019-12541-7, 2019.

Weiss, R. F. and Price, B. A.: Nitrous oxide solubility in water and seawater, Mar. Chem., 8, 347–359, https://doi.org/10.1016/0304-4203(80)90024-9, 1980.

Wesslander, K., Omstedt, A., and Schneider, B.: Inter-annual and seasonal variations in the air–sea CO_2 balance in the central Baltic Sea and the Kattegat, Cont. Shelf Res., 30, 1511–1521, https://doi.org/10.1016/j.csr.2010.05.014, 2010.

Wesslander, K., Hall, P., Hjalmarsson, S., Lefevre, D., Omstedt, A., Rutgersson, A., Sahlée, E., and Tengberg, A.: Observed carbon dioxide and oxygen dynamics in a Baltic Sea coastal region, J. Marine Syst., 86, 1–9, https://doi.org/10.1016/j.jmarsys.2011.01.001, 2011.

Wiesenburg, D. A. and Guinasso, N. L.: Equilibrium solubilities of methane, carbon monoxide, and hydrogen in water and sea water, J. Chem. Eng. Data, 24, 356–360, https://doi.org/10.1021/je60083a006, 1979.

Woolf, D. K., Land, P. E., Shutler, J. D., Goddijn-Murphy, L. M., and Donlon, C. J.: On the calculation of air-sea fluxes of CO_2 in the presence of temperature and salinity gradients, J. Geophys. Res.-Oceans, 121, 1229–1248, https://doi.org/10.1002/2015JC011427, 2016.

Yurkovskis, A., Wulff, F., Rahm, L., Andruzaitis, A., and Rodriguez-Medina, M.: A Nutrient Budget of the Gulf of Riga; Baltic Sea, Estuar. Coast. Shelf S., 37, 113–127, https://doi.org/10.1006/ecss.1993.1046, 1993.